ISRN LUTMDN/TMHP-15/5337-SE

ISSN 0282-1990

3D-modeling of swing check valve with connection to dynamic behavior used in system studies

Christoffer Björk

Thesis for the degree of Master of Science in Mechanical Engineering
Division of Fluid Mechanics
Department of Energy Sciences
Faculty of Engineering | Lund University

This degree project for the degree of Master of Science in Mechanical Engineering has been conducted at the Division of Fluid Mechanics, Department of Energy Sciences, Faculty of Engineering, Lund University and at TÜV NORD Sweden AB.

Supervisor at the Division of Fluid Mechanics was Prof. Johan Revstedt.
Supervisor at TÜV NORD Sweden AB was Dr. Faruk Selimovic.
Examiner at Lund University was Prof. Bengt Sundén.

The project was carried out in cooperation with TÜV NORD Sweden AB.

Thesis for the Degree of Master of Science in Mechanical Engineering

ISRN LUTMDN/TMHP-15/5337-SE

ISSN 0282-1990

Division of Fluid Mechanics
Department of Energy Sciences
Faculty of Engineering, Lund University
Box 118, 221 00 Lund
Sweden
www.energy.lth.se

Abstract

This Master's Thesis is the result of the collaboration between The Technical Faculty of Lund University and TÜV NORD Sweden AB. Focus has been directed towards the nuclear industry where this thesis is one of several other Master's Theses regarding the dynamic modeling of a swing check valve.

It is necessary for the nuclear industry to be able to model flow transients which involve the dynamic behaviour of the swing check valve. The modeling is commonly executed by one-dimensional codes such as RELAP5, DRAKO and DYVRO. This work has applied the swing check valve theory by (Li and Liou, 2003) in order to retrieve results from three-dimensional modeling using computational fluid dynamics (CFD) to derive useful correlations for one-dimensional code implementation.

The accuracy of the CFD-model has been investigated by comparing results of interest after changing the modeling set-up in the CFD-software ANSYS FLUENT. The impact of cell density, solver dependence and choice of turbulence model are a couple of interesting preferences which have been investigated in a sensitivity analysis. The simulations are constructed to yield results for useful parameters for the swing check valve theory.

Results from CFD-simulations give resembling results compared to the experiments by (Li and Liou, 2003). One particular correlation was found regarding the coupling of the coefficients in the theory of (Li and Liou, 2003) and was implemented in RELAP5. Through this work conclusions has been made that the implementation of a general one-dimensional model based on the theory of (Li and Liou, 2003) will be complex due to coefficient dependence.

Zusammenfassung

Diese Masterarbeit ist ein Ergebnis der Zusammenarbeit zwischen der Technischen Fakultät der Universität Lund und TÜV NORD Sweden AB. Fokus ist auf die Kernkraftindustrie, wo diese Arbeit ist eine von mehreren anderen Masterarbeiten in Bezug auf die dynamische Modellierung einer Rückschlagklappe gerichtet.

Es ist notwendig für die Kernindustrie in der Lage, transiente Strömung, die das dynamische Verhalten des Rückschlagventils beinhaltet modellieren. Die Modellierung wird häufig durch eindimensionale Codes wie RELAP5, DRAKO und DYVRO ausgeführt. Diese Arbeit hat die Rückschlagklappe Theorie von Li und Liou, um die Ergebnisse aus dreidimensionalen Modellierung mit Computational Fluid Dynamics (CFD), um nützliche Korrelationen für eindimensionale Codeimplementierung abzuleiten abrufen verwendet.

Die Genauigkeit der CFD-Modell wurde von den Vergleich der Ergebnisse von Interesse nach der Änderung der Modellierung Set-up in der CFD-Software ANSYS FLUENT gesucht. Der Einfluss der Zelldichte, Löser Abhängigkeit und die Wahl der Turbulenzmodell gibt eine Reihe von interessanten Eigenschaften, die in einer Sensitivitätsanalyse untersucht geworden sind. Die Simulationen werden eingestellt, um nützliche Ergebnisse für die Rückschlagklappe Theorie ergeben.

Ergebnisse von CFD-Simulationen gaben ähnlichen Ergebnissen im Vergleich zu den Experimenten, die von Li und Liou sind. Eine bestimmte Korrelation wurde hinsichtlich der Kopplung der Koeffizienten in der Theorie von Li und Liou gefunden. Durch diese Arbeit hat Schlussfolgerungen gemacht, dass die Umsetzung einer allgemeinen eindimensionalen Modells werden komplex sein aufgrund der Koeffizient Abhängigkeit

Acknowledgements

I would like to express my gratefulness to my supervisor Dr. Faruk Selimovic at TÜV NORD Sweden for his guidance and expertise through this thesis. Equally so, I would like to thank Martin Turesson at TÜV NORD Sweden for all his useful thoughts and discussions during this thesis. I would also like to thank Onsala Ingenjörsbyrå AB for their assistance in running CFD-simulations when time grew short.

I would also like to thank my academic supervisor Prof. Johan Revstedt at the Technical Faculty of Engineering at Lund University for his inputs and support regarding CFD during this thesis and for introducing me to the inspiring world of CFD.

Finally, I would like to thank my wonderful family and friends for all their love and support.

Christoffer Björk
Helsingborg, June 2015

Nomenclature

A	Area
c	Acoustic velocity
F	Force
D	Diameter
g	Gravitational acceleration
L	Length
I	Inertia
Δp	Differential pressure
r	Distance to rotational axis
Q	Volumetric flow rate
T	Torque
t	Time
v	Velocity
y^+	Dimensionless wall distance

δ_{ij}	Kroeneker delta
ϵ	Dissipation of turbulent kinetic energy
θ	Opening angle
$\ddot{\theta}$	Angular acceleration
μ	Dynamic viscosity
ν	Kinematic viscosity
ν_T	Turbulent viscosity
ρ	Density
σ_k	Prandtl number
τ_{ij}	Viscous stress tensor
$\dot{\theta}$	Angular velocity

Contents

List of Figures

List of Tables

1 Introduction

1.1 Background

It is of great importance in the nuclear industry to be able to model flow transients to determine hydraulic loads within various pipe systems. The hydraulic loads will result in stresses which can cause severe damages on pipe systems or on single components. To ensure the highest possible safety, flow transients within pipe systems are modeled to ensure that the system can withstand and cope with these loads. The hydraulic loads initially starts to propagate due to change in pressure within the system. Pressure changes can occur due to pump stops or due to opening and closure of valves. These events often involve back flow, which means that the flow changes direction and travels upstream.

Back flow can be prevented or greatly reduced by a check valve. Check valves are commonly used in nuclear power plant applications, mainly due to design features, size variation, favorable pressure drop and economy. Check valves are one of few valve models which can operate without external control. A swing check valve commonly consists of a disc connected to a hinge pin above the flow stream inside the valve housing. The most basic function of a check valve is to allow throughflow in one direction and prevent throughflow in the opposite. This property is especially of value when reversed flow is undesirable and should be minimized. Further detailed reviews on different check valves can be found in (Zappe and Smith, 2004) and (McElhaney, 2000). A cross section illustration of a typical swing check valve can be seen in Fig 1.1.

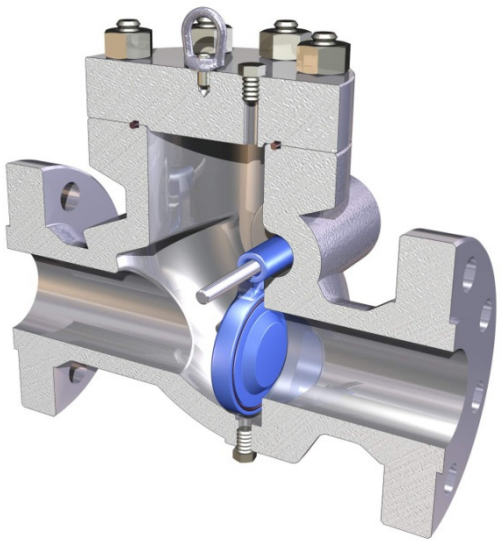

Figure 1.1: Cross sectional view of a typical swing check valve.

Even though preventing back flow appears to be a trivial matter, the effects of operable valves are definitely taken into the system calculations when designing pipe systems. This is mainly due to the risk of pressure surges associated with the closure process. These pressure surges are also known as water hammers and

generally occur when a fluid is suddenly forced to stop or to change direction. The resulting pressure wave propagates through the system with the local speed of sound and can be reflected multiple times until the friction losses reduce the kinetic energy which leads to dissolving. This phenomena can expose the system to extreme hydraulic loads which can lead to severe damages including pipe rupture.

It is desirable to efficiently model the behavior of check valves to predict pressure surges and the magnitude of back flow. An efficient approach used in the nuclear industry is to use one-dimensional models as predictors. These modes are often based on well known physics governed by Newton's laws. The difficulty with these models is to couple the hydraulic forces from the fluid affecting the moving disc of the valve. This coupling is often the most significant difference between existing one-dimensional models and will be investigated in this work.

In 2003, a new fundamental approach regarding the implementation of the governing equation of motion was presented by Guohua Li and Jim C. P. Liou. The modeling of throughflow and valve motion coupling was presented in an new innovative manner, unlike previous theories. The new torque model separates the torque caused by the throughflow into two additive components, one stationary and one rotational component. The close matching between the results from the numerical simulations and the laboratory data demonstrated the validity of the proposed approach to swing check valve characterization. The theory by (Li and Liou, 2003) has previously been investigated through CFD-simulations by (Boqvist, 2013), where it was confirmed that CFD-simulations can provide resembling results from the experiments. This is an incitement to further strive and develop a one-dimensional model based on this theory. In the Master's Thesis by (Turesson, 2011), it was investigated how a number of current one-dimensional swing check valve models behave in compression with a CFD-model. It was shown that all one-dimensional models under predicts the closing time. The work by (Turesson, 2011) include the determination of a important coefficient used in the theory of (Li and Liou, 2003).

1.2 Objectives

The theory of (Li and Liou, 2003) will be taken into consideration as three dimensional CFD-simulations will provide data in order to facilitate the development of a one-dimensional swing check valve model. To be able to reach this stage, an existing CFD-model will be improved in order to maximise the performance during transient flow scenarios. The thesis will present a thorough review on the theoretical approach of (Li and Liou, 2003) and how the theory can be modified in order to set up a suitable CFD-approach.

1.3 Thesis outline

The main reason why it is of interest to model the physics and phenomena regarding a swing check valve is to master the control of pressure surge and back flow in pipe systems. Hence the contents of this thesis will consciously follow the link between valve closure and pressure surge. The important physics controlling the motion of the swing check valve is early introduced.

The innovative theory of (Li and Liou, 2003) will be the foundation during the CFD-simulations and one-dimensional correlations. Hence the theory will be thoroughly reviewed in order to understand how the implementation will differ between experimental- and CFD-implementation.

Since the work involve a comprehensive amount of CFD-simulations, a proper presentation of relevant CFD-theory will be included in the theory section. Hence, the coupling between CFD-theory and the CFD-model will be be facilitated when the model is presented in the method section. This section includes the description of the model construction and how the model is implemented in ANSYS FLUENT. Important approaches and settings used in ANSYS FLUENT will be presented in order to demonstrate how CFD can be used for real industrial problems.

The result section will begin with reviewing the retrieved data through the sensitivity analyses. These results will be determining how further CFD-simulations are executed. The remaining part of the result section will include useful results according to the theory of (Li and Liou, 2003) and a presentation of the derived correlations. The result section ends with a presentation of the results retrieved from

implementation in RELAP5. The results will be discussed and conclusions will be presented. The thesis ends with suggestions for future work.

1.4 Assumptions and limitations

- CFD-simulations will only be performed on the available model provided by TÜV NORD Sweden. The model will however be revised and improved. Stationary simulations will be performed on a certain amount of different opening angles, where quantities for non-calculated angles will be interpolated. The same applies for number of different velocities and flow decelerations in stationary and transient cases.
- During stationary simulations, the fluid domain will only consist of incompressible water which will allow changes at the boundaries to propagate through the domain at an instant. For the transient simulations compressible water is used to improve the conditions of calculating Joukowsky surges as a result of valve closure.
- No two-phase flows as a result of valve closure will be investigated. Hence, the flow domain of the CFD-model will only consist of water. Phenomena such as column separation and vapor generation will not be investigated.

2 Theory

This section includes the theory on which this work is based on. The very fundamental physical correlations of Newton will be used as take-off and will more or less be implemented in all further theory. Newtons law of motion is the governing relationship between the forces acting on the valve and its responsive motion. The motion of the valve is affected by a number of different forces and corresponding torques, which have been modeled with different approaches in different theories. This work will use the theory of (Li and Liou, 2003) to investigate how to develop a one-dimensional model. This makes it suitable to present a enhanced review to really understand the theory and how it will be implemented in this work. In addition to the work of (Li and Liou, 2003) the work of (Pandula and Halász, 2002) will be reviewed in order to present a different approach in modeling a rotating valve.

All experiments in this work will be computational experiments executed with the theory governing computational fluid dynamics. The CFD-theory is vast since it is a fusion between theory of numerics, fluid mechanics and heat transfer. Hence the presented theory of CFD will include problem specific theory which will be used in the CFD-software ANSYS FLUENT.

A theoretical description of the swing check valve model used in three known one-dimensional codes RELAP5, DRAKO and DYVRO will be presented. The swing check valve model is just one component which can be connected to a system of pipe and other components in these one-dimensional codes.

2.1 Physics of rotational motion

Newton laws of motion are used to describe the forces which governs the motion of the swing check valve. Newtons second law of motion in terms of an objects acceleration can be expressed as in Eq. 2.1.

$$\mathbf{F} = m\frac{d\mathbf{v}}{dt} = m\mathbf{a} \tag{2.1}$$

Here $\mathbf{F}$ is the net force acting upon the object and m the mass of the object. The magnitude of acceleration of an object is directly proportional to the net force and inversely proportional to the mass of the object. The second law of motion can be applied on the center of mass of an object rotating around a principal axis which in simple cases is a symmetry axis. Consider an object with the mass m, rotating in a circle at the radius r. The object is accelerated by a tangential force F_t. The acceleration from the second law of motion on the tangential can be expressed as in Eq. 2.2.

$$a_t = r\ddot{\theta} \tag{2.2}$$

The torque caused by the rotational force F_t at the distance r from the center of rotation is expressed in Eq. 2.3.

$$T = F_t r \tag{2.3}$$

Hence the rotational torque can be expressed by the mass of the object and the angular acceleration using Eq. 2.2 and Eq. 2.3.

$$T = F_t r = m a_t r = m r^2 \ddot{\theta} = I\ddot{\theta} \tag{2.4}$$

Here I is the rotational inertia and $\ddot{\theta}$ is the angular acceleration. By summarizing mass increments of an object, a rigid body motion can be expressed according to Eq. 2.5.

$$\sum T = \sum I\ddot{\theta} \quad \Leftrightarrow \quad T_{tot} = I_{tot}\ddot{\theta} \tag{2.5}$$

Here T_{tot} is the net external torque and I_{tot} is the total rotational inertia. The implementation of the torque terms in T_{tot} vary for different swing check valve theories and will be partly presented in section 2.2.1 and section 2.2.2. The rotational inertia is the resistance within the system to change the rotation of that system. The rotating motion of a swing check valve is not around its center of gravity. Hence the parallel axis theorem, also called Huygens–Steiner theorem can be applied to determine the rotational inertia around any axis. This expression also states that the minimum rotational inertia is around an axis through the center of mass (Nyberg, 2010).

$$I = I_{cm} + md^2 \tag{2.6}$$

The rotational inertia can be expressed for all bodies according to Eq. 2.7.

$$I_{tot} = \sum m_i r_i^2 = \int_M r^2 dm = \int_V \rho r^2 dV \tag{2.7}$$

The rotational inertia is additive and can be summarized by the rotational inertia of the different components of a simplified swing check valve. Their rotational inertia is determined by their geometry and mass. The individual rotational inertia of the moving parts of the valve are presented in Eq. 2.8 and Eq. 2.9 using the parallel axis theorem.

$$I_{disc} = \frac{1}{4} m_{disc} R_{disc}^2 + m_{disc} L_{disc}^2 \tag{2.8}$$

$$I_{rod} = \frac{1}{12} m_{rod} L_{rod}^2 + m_{rod} \left(\frac{L_{rod}}{2} \right)^2 \tag{2.9}$$

As the valve disc is submerged in water it will accelerate a certain amount of surrounding fluid. The amount of this fluid has an inertia that in some cases need to be considered when determine the torque. According to (Thorley, 1989) this inertia can be approximated by adding the inertia of a fluid sphere with the same diameter as the valve disc. This inertia is presented in Eq. 2.10 using the parallel axis theorem.

$$I_{sphere} = \frac{2}{5} m_{fluid,sphere} R_{disc}^2 + m_{fluid,sphere} L_{disc}^2 \tag{2.10}$$

2.2 Modeling of rotating check valve

Two different theories regarding the modeling of a rotating valve will be presented. The work of (Li and Liou, 2003) focuses on a swing check valve, while the work of (Pandula and Halász, 2002) focuses on a tilting disc valve. The fundamental difference between the theories is the modeling of the hydraulic torque caused by the flow. This torque is caused by the pressure difference around the valve disc. Due to complicated flow patterns around the valve disc, it is difficult to measure the pressure distribution analytically or by experiments which is why different theories have been developed to estimate this torque.

2.2.1 Theory by G. Li and J. C. P. Liou

The primary theoretical innovation in the work by (Li and Liou, 2003) is the modeling of the hydraulic torque component which will be presented together will all other torque components used in Eq. 2.5. The angular momentum equation in the work of (Li and Liou, 2003) is presented in Eq. 2.11.

$$T_{tot} = T_{hydraulic} + T_{weight} + T_{friction} + T_{external} = (I + I_E + I_f)\ddot{\theta} \tag{2.11}$$

As seen in Eq. 2.11, the torques which determines the rotational motion are the torque caused by throughflow, weight, friction and the external coupled devices. The inertia in Eq. 2.11 is the inertia of the disc, external coupled devices and added mass. It is important to state that the expressions in the article by (Li and Liou, 2003) is derived from experiments which makes a computational set up in CFD different due to the possibilities to neglect and calculate certain properties directly. The authors state that friction is less important for larger valves where the valve used in this thesis is approximately 97% larger than the valve used in the experiments by the authors. This statement determines the neglecting of friction. The valve model does not include an external coupled device which allows $T_{external}$ to be neglected.

Weight torque

The torque caused by weight is the resulting torque that is determined by the weight of the submerged valve disc and the effective lever arm between the center of mass of the valve disc and the pivot point. The weight of the submerged valve disc is determined by the two contributions, gravitational force and buoyancy force. The gravitational force will tend to close the valve, where in contrary the buoyancy force will expose the valve to a lifting force, corresponding to the weight of the displaced fluid. This phenomena is also known as Archimedes' principle. In the work of (Li and Liou, 2003) a horizontal mounted swing check valve was used. The resulting torque of weight is modeled according to Eq. 2.12.

$$T_{weight} = -(m_{valve\,disc} - m_{fluid})gL_{cg}sin(\theta) \tag{2.12}$$

Here L_{cg} is the distance between the hinge pin and the center of mass of the valve disc and θ is the opening angle. The torque due to weight will be maximized when the valve is fully open. The torque decreases proportional to the sine-function of the opening angle. The trigonometric function is determined by the mounting of the check valve, i.e. the rotational direction of the lever arm relative the opening angle. The expression for weight torque for a check valve mounted in a vertical pipe should include a cosine-term according to Eq. 2.13. An illustration of the weight torque is presented in Fig. 2.1.

$$T_{weight} = -(m_{valve\,disc} - m_{fluid})gL_{cg}cos(\theta) \tag{2.13}$$

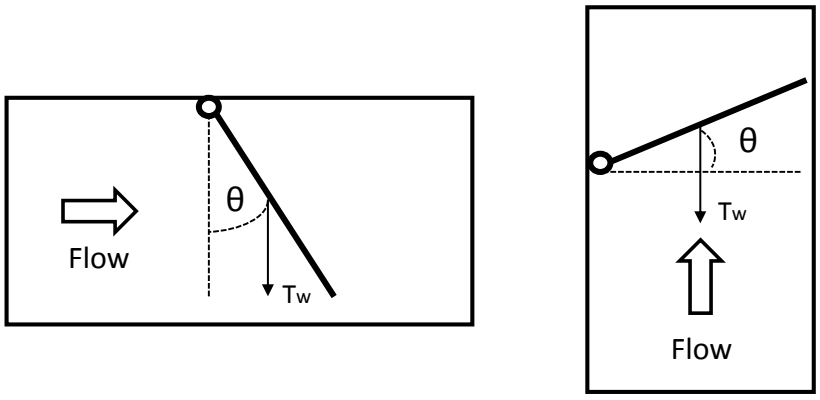

Figure 2.1: Weight torque for horizontal and vertical mounted swing check valve.

Hydraulic torque

One of the fundamental differences compared to other swing check valve models is the separation of the hydraulic torque. The hydraulic torque is separated into two additive torque components, one regarding the torque acting on a fix disc and one regarding a moving disc where the pressure distribution changes and creates an additional torque. These two torque components act independently and can act in both clockwise and counterclockwise direction depending on the direction of through flow and rotational direction of the valve disc. The summarized hydraulic torque is presented in Eq. 2.14.

$$T_H = T_{HS} + T_{HR} \tag{2.14}$$

The two resulting torque terms is the stationary hydraulic torque T_{HS} and the rotational hydraulic torque T_{HR}. The stationary hydraulic torque has been defined as seen in Eq. 2.15

$$|T_{HS}| = C_{HS}\rho A_v \frac{V^2}{2} L \tag{2.15}$$

The stationary hydraulic torque resembles the the common expression for drag, often used in aerodynamic calculations (Young et al., 2007). If the drag force is causing an object to rotate about an axis the expression for this torque can be expressed as:

$$T_{drag} = \frac{1}{2} C_d \rho A_p V^2 L \tag{2.16}$$

The stationary hydraulic torque coefficient C_{HS} is assumed to handle the the angle dependency which can be seen by the difference in used area between Eq. 2.15 and Eq. 2.16 where the drag is based on the projected area. The definition of the rotational torque component is presented in Eq. 2.17.

$$|T_{HR}| = C_{HR}\rho A_v \frac{(L\dot{\theta})^2}{2} L \tag{2.17}$$

Both equations for stationary- and rotational hydraulic torque include the fluid density ρ, the disc area A_v and the distance between the hinge pin and the disc center L. The flow velocity at the valve seat V and the stationary hydraulic torque coefficient C_{HS} is also included in the term for stationary hydraulic torque. The coefficient C_{HS} said to be dependent of opening angle and direction of flow and is assumed to be independent of flow velocity. The rotational hydraulic torque component include the angular velocity of the valve disc $\dot{\theta}$ and a rotational hydraulic torque coefficient C_{HR}. Hence, it is a dynamic term which is said to be a function of disc angle, angular velocity and the magnitude and direction of through flow. An important effect of T_{HR} is that it prevents premature closure compared to other numerical models, according to (Li and Liou, 2003). The magnitude is increased for small angles.

In the experiments by (Li and Liou, 2003) the stationary hydraulic torque coefficient is derived by maintaining the disc at at different angles by controlling the through flow. The through flow is gradually increased and decreased to produce a upswing and downswing of the disc during forward and backward flow. The external torque T_e counteracts the stationary hydraulic torque and is used to balance the disc at fixed position. At the very moment just before the disc starts to move either up- or down the frictional torques are assumed to be equal and can therefore be eliminated. This is based on the conclusion that the magnitude of the static frictional torque is equal and independent of rotational direction. This yields the following expression which is used by the authors to describe the stationary torque coefficient.

$$C_{HS} = \frac{2(T_w + T_E)}{\rho A_v V^2 L} \tag{2.18}$$

Since it it possible to directly calculate the hydraulic torque using CFD, the stationary hydraulic torque coefficient can be derived only using Eq. 2.14 and Eq. 2.15 neglecting the rotational hydraulic torque due to the absence of valve disc motion. The equation for the stationary hydraulic torque coefficient for CFD-simulations is presented in Eq. 2.19.

$$C_{HS} = \frac{2T_{HS}}{\rho A_v V^2 L} \tag{2.19}$$

The hydraulic rotational torque component T_{HR} is always positive during closure, which means that it opposes the direction of the closing valve and acts as a breaking torque in the counter clockwise direction. The stationary torque component T_{HS} always acts in the same direction as the through flow. Hence, T_{HS} changes sign as the through flow changes direction. In Eq. 2.20, the external torque T_E counteracts the static hydraulic torque since it it used to balance the valve disc. The kinetic friction term T_{FK} is also included in the derived expression used by the authors to describe the rotational hydraulic torque coefficient.

$$C_{HR} = \frac{|T_w| \pm |T_{HS}| - |T_{FK}| \pm |T_E| + I_{tot}\ddot{\theta}}{\frac{1}{2}\rho(L\dot{\theta})^2 A_v L} \tag{2.20}$$

Equation 2.20 can be clarified using a plane divided into four quadrants with through flow on the vertical axis and angular velocity of the valve disc on the horizontal axis. Positive throughflow direction is considered downstream and positive rotational direction is considered counter clockwise, i.e. an opening motion of the valve disc. Figure 2.2 show that the stationary hydraulic torque component should be positive in quadrant 1 and 2, where the through flow is positive, i.e. directed downstream. The rotational hydraulic torque component has different sign in these quadrants due to dependence of the direction of angular velocity. Since the rotational hydraulic torque component is negative in quadrant 1, it counteracts the opening motion of the valve disc and acts as a dampening torque. The rotational hydraulic torque component has the same sign as the stationary hydraulic torque in quadrant 2, where the valve is closing in forward throughflow. This quadrant resembles the early stage of a check valve closure during system shut down. The hydraulic torque terms have different signs in quadrant 3, where the valve is closing during backward flow. This quadrant resembles the late stage of check valve slam. Quadrant 4 is without torque terms and resembles an opening valve disc during back flow which is unlikely to occur in reality.

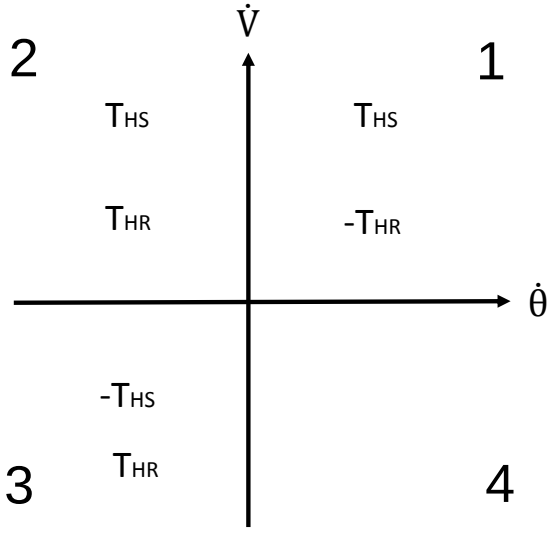

Figure 2.2: Arrangement of the two hydraulic torque components with respect to direction of flow and direction of angular velocity.

The same approach used in Eq. 2.19 is used to derive a suitable expression for calculating the rotational hydraulic coefficient with CFD. Hence, Eq. 2.14 and Eq. 2.17 gives the following equation.

$$T_H = T_{HS} + C_{HR}\rho A_v \frac{(L\dot{\theta})^2}{2} L \quad \Rightarrow$$

$$C_{HR} = \frac{T_H - T_{HS}}{\rho A_v \frac{(L\dot{\theta})^2}{2} L} \tag{2.21}$$

The contribution of rotational inertia due to the approximated accelerated sphere of fluid to the total rotational inertia is often important for one-dimensional modeling. However, it is assumed that CFD-simulations will handle this inertia through the implementation of the two coefficients C_{HS} and C_{HR}.

2.2.2 Theory of Z. Pandula and G. Halász

The incitement of the presentation of the theory of (Pandula and Halász, 2002) is to demonstrate a quite different approach in modelling a rotating valve. The modeling is directed towards pipe planning where the mathematical check valve model is constructed to simulate check valve behaviour at full closure and at change of flow conditions in pipes. The theory is developed by experiments on a tilting disc valve, which is a different kind of check valve compared to the swing check valve. A typical tilting check valve can be seen in Fig. 2.3. The angular momentum equation is based on Eq. 2.5 and is expressed in Eq. 2.22.

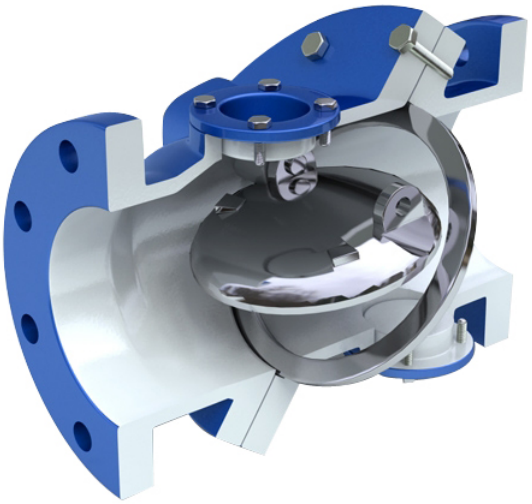

Figure 2.3: Cross sectional view of a typical tilting disc valve.

$$T_C + T_{massload} + T_{hydraulic} + T_{breaking} + T_{damping} + T_{friction} = I_{tot}\ddot{\theta} \tag{2.22}$$

The torque caused by weight of the valve disc is divided into two components where the angle dependence is handled by a coefficient in the expression for torque caused by eccentricity T_C. This torque component is presented in Eq. 2.23.

$$T_C = -K_C(\theta)m_0 gD \tag{2.23}$$

Here K_C is the angle dependent coefficient, m_0 is mass of the valve disc and D is the nominal diameter of the valve disc. The second torque component is the torque caused by the actual mass load of all the rotating parts of the valve. Compared to the theory of (Li and Liou, 2003), this torque component is modeled without any trigonometric function and is presented in Eq. 2.24.

$$T_{massload} = -L_{cg}mg \tag{2.24}$$

Here L_{cg} is the length of the lever arm and m is the mass of all rotating parts. The damping torque $T_{damping}$ represents the damping effect of viscous oil, possibly within the bearings of the valve. It is dependent on opening angle and direction and magnitude of angular velocity. The damping torque is presented in Eq. 2.25.

$$T_{damping} = \begin{cases} K_b(\theta)\dot{\theta}^2 & \dot{\theta} < 0 \\ 0 & \dot{\theta} \geq 0 \end{cases} \tag{2.25}$$

The torque caused by friction $T_{friction}$ is said to have a relatively high influence on the rotating shaft, which is why this torque is included and based on the materials of the bearings, mass of the rotating parts, mass load and pressure drop. This torque component is presented in Eq. 2.26.

$$T_{friction} = \mu \frac{d_t}{2} \sqrt{[(m + m_0)g + \Delta pAsin(\theta + \theta_s)]^2 + [\Delta pAcos(\theta + \theta_s)]^2} \tag{2.26}$$

The friction torque is modeled according to Coloumb's law where μ is the friction coefficient of the bearing material. The two squared terms are the horizontal and vertical force components of the normal force on the bearings. The normal force consists of the vertical force due to gravity, the vertical component of the resulting force due to pressure difference across the valve disc and corresponding horizontal force. The term $\frac{d_t}{2}$ is the inner radius of the bearings, acting as lever arm.

The breaking torque $T_{breaking}$ is caused by the the viscous fluid streaming against the valve disc and opposes the direction of closure, same as the rotational hydraulic torque in the theory of (Li and Liou, 2003). However, the modeling is is quite different.

$$T_{breaking} = -\rho \left(\frac{D^5}{60} + \frac{D^2}{2} e^2 \right) \dot{\theta}|\dot{\theta}| - \frac{2}{3} \rho D^3 e \dot{\theta} v cos(\theta + \theta_s) \tag{2.27}$$

Here $\dot{\theta}$ is the angular velocity, e is the eccentric distance and v is the fluid velocity. The development of the model of this torque component is based on theoretical considerations and has been customized to suit the swing check valve model used in the one-dimensional code DYVRO.

2.3 Pressure surge and water hammer

Pressure surge is commonly referred as water hammer due to the characteristic noise of a water column that has been brought to rest at an instant, often within in pipe systems. This section explains why and how certain actions can result in pressure surges, both theoretical and in practice. The theory of pressure surges will be taken into consideration when the CFD-model is developed and used.

2.3.1 Theory

A fluid flow within a closed conduit, e.g. a pipe, that experiences a distortion induces a corresponding change in pressure. This is due to the change in momentum of the fluid. The changes in pressure caused by this dependence are called waterhammer (Záruba, 1993). Small distortions may not cause any noteworthy pressure changes, however, large changes in the system may cause serious loads. The most essential expression for describing the magnitude of pressure surges in relation to velocity changes is the Joukowsky equation. This equations determines the maximum pressure rise due to the disruption of flow. The pressure surge travels at the acoustic speed through the pipe system, conveying the pressure rise. Depending on the deceleration of the fluid during the time of disruption, the magnitude of the pressure surge is determined. The Joukowsky equation can only be applied during at which the change in velocity takes place. The simple expression for the rise in pressure is presented in Eq. 2.28.

$$\Delta p = \rho c \Delta u \tag{2.28}$$

The equation states that the magnitude of the pressure surge, Δp depend on the density of the fluid, ρ, the wave propagation speed which is the acoustic velocity, c, and the magnitude of change in velocity, $\Delta u = u_1 - u_2$. The magnitude of reversed velocity and the acoustic wave speed are the terms which have the largest impact on the pressure surge. If the flow is brought to rest, Δu will be maximized, and hence the pressure surge as well. However, the use of the Joukowsky equation is also restricted to the closing interval Δt. It is necessary to demonstrate at what conditions the Joukowsky surges apply. The appliance will later be explained by a simplified case where fluid flows from a reservoir through a horizontal pipe, where the volume flow rate is controlled by a valve fixed downstream of the reservoir, illustrated in Fig. 2.5.

An incompressible fluid flows through a frictionless pipe at a certain velocity with a certain inertia until it encounter a disruption in the flow path. In reality this disruption can be caused by change of pump conditions or by valve closure (KSB, 2006). If the discharge changes linearly with time, the pressure is distributed through the pipe as seen in Fig. 2.4.

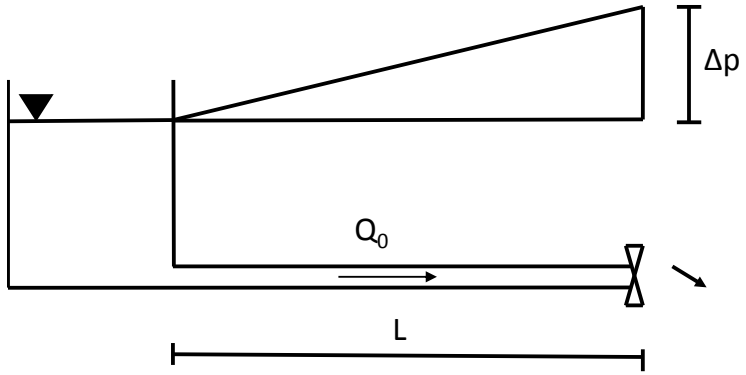

Figure 2.4: Pressure distribution due to linear discharge.

The fluid is unable to adjust to the new conditions instantaneously which result in a change in momentum of the liquid that is equal to the momentum caused by the pressure difference between the upstream and downstream end of the pipe during the time interval Δt (Záruba, 1993), expressed in Eq. 2.29.

$$AL\rho\frac{Q_0}{A} = \Delta pA\Delta t \tag{2.29}$$

Here A is the cross sectional area of the pipe, L is the length of the pipe, ρ is the density of the fluid and Q_0 is the initial volume flow rate. The velocity of the flow, v_0, is the volume flow rate divided by the cross sectional area and it can be used to express the pressure difference according to Eq. 2.30.

$$\Delta p = \frac{L\rho v_0}{\Delta t} \tag{2.30}$$

The closing interval must be put in relation with the pipe period, $T = 2Lc$, which is defined as the time taken for a restoring reflection to arrive at the source of the initial transient propagation (Douglas et al., 2005). If the closing interval of the valve is sufficiently long, $\Delta t >> T$, Eq. 2.30 is valid. When the closing interval is small compared to the pipe period, $\Delta t << T$, the closing can be considered abrupt. From a theoretical point of view, it is important to observe a scenario which involve an instant closing where $\Delta t \Rightarrow 0$, which would lead to an infinite pressure rise according to Eq. 2.30. This makes Eq. 2.30 invalid. The unrealistic event is prevented by the effects of pipe elasticity and fluid compressibility. If the fluid is assumed to be compressible during an abrupt closure, the generated pressure change will propagate through the pipe at the acoustic velocity c. The stationary initial fluid flow will be brought to rest at the same velocity as the propagating pressure wave. The distance traveled by the pressure wave at time t is expressed in Eq. 2.31.

$$\Delta x = ct \tag{2.31}$$

Here c is the acoustic speed in the fluid medium. This correlation is used in a different form of Eq. 2.29, where the pipe length L and time interval Δt has been replaced by the actual traveled distance by the wave Δx and the corresponding time t.

$$A\Delta x\rho\frac{Q_0}{A} = \Delta pAt \quad \Rightarrow \quad \Delta p = c\rho v_0 \tag{2.32}$$

Equation 2.32 can be clarified by considering a simplified system which consists of a reservoir and a valve connected by a pipe. The fluid flows from the reservoir through the open valve. As the valve closes instantly, an induced pressure wave propagates upstream towards the reservoir, increasing the pressure

in the pipe, as seen in Fig. 2.5 a. Figure 2.5 b shows how the pressure wave has traveled upstream and pressurized the entire upstream pipe. When the wave strikes the orifice of the reservoir, it reflects due to the abrupt area change of the much larger reservoir. This reflected pressure wave reduces the pressure rise in the pipe to its initial level as it travels downstream towards the valve, as seen in Fig. 2.5 c. Since pressure between the wave and valve is higher than the pressure between wave and reservoir, fluid flows upstream into the reservoir. As the restoring wave reaches the valve, there is no remaining fluid ahead to support the reversed flow which yields a low pressure region and a pressure-reducing wave, seen in Fig. 2.5 d. The behavior of the reflecting pressure waves can be compared to how waves behave when encountering a wall or an open orifice. Once again, the pressure wave propagates towards the upstream reservoir, changes direction and resets the low pressure region in the pipe. Since the wave propagation time is limited to the length of the pipe and to the acoustic wave speed, this restoring pressure wave can not reach the source of the transient in less than one pipe period, T. This increment of time is the longest time a valve can be closed and still cause a pressure rise equal to an instant closure (Tullis, 1989). As seen in Fig. 2.5, the transient pressure distribution is displaced one pipe period compared to the downstream pressure distribution. It is assumed that the pressure drop is insufficient to lower the pressure below vapour pressure. Wave propagation like the described example would continue for an infinite period of time without the influence of friction. Friction would damp the pressure oscillations within a short period of time in practise.

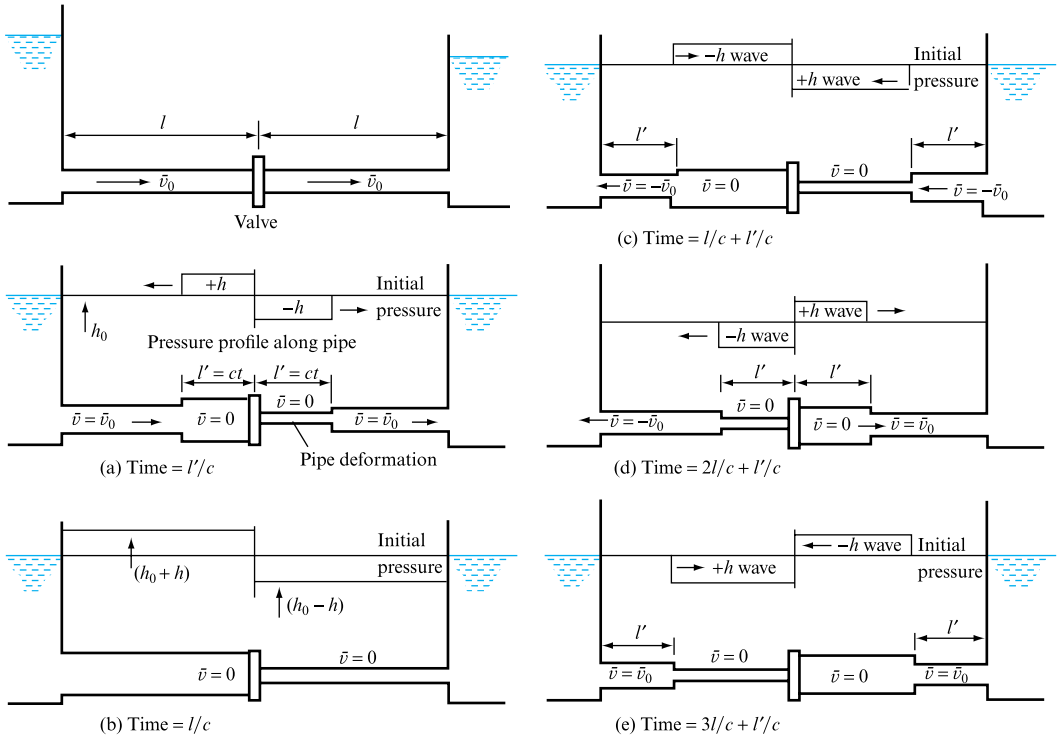

Figure 2.5: Schematic figure of pressure surge propagation (Douglas et al., 2005).

The Joukowsky equation takes its form when considering linear change in discharge during a closure interval comparable to the same length of time as the pipe period. The increments in change in flow ΔQ due to closure increment over a time interval Δt corresponds to the pressure change Δp (Záruba, 1993).

$$\Delta p = \frac{\rho c}{A} \Delta Q = \rho c \Delta v \tag{2.33}$$

It seems contradictory to claim that no pressure surge have been generated if valve closure occur in less time than a pipe period, even though the wave already have propagated during a pipe period. The answer is that this is a mathematical interpretation of how pressure surges are generated and propagates due to change in momentum of the fluid and does not necessary happen in reality.

A swing check valve can not perform an instant closure in reality. However, as back flow often occur at

the later part of the closure process the flow will accelerate the valve disc to its seat. This final closure can be faster than a pipe period and can therefore be considered instant. The rise in pressure due to the final closure can be summarized by the contributions of the final closure seen as a number of incremental closures, equal to Δp (Tullis, 1989). This states that the rise in pressure would be the same as if the swing check valve where to close instantaneously.

If no back flow occurs the valve will close smoothly as it copes with the flow during pressure decrease. Hence no pressure surge, i.e. the pressure surge does not depend on the closing time of the valve, it is the magnitude of back flow that has a large impact on the level of pressure surge. The most desirable scenario is a fast valve closure with no back flow. The mechanical slam of the valve against the seat does not cause pressure surge within the fluid, only in the mechanical structure of valve and pipe system.

2.3.2 Causes of pressure surges

Any operation which can cause a rapid change in flow velocity can result in propagating pressure surges. The following operations are examples of real transients in different pipe systems (Tullis, 1989).

- Change of valve opening.
- Change in pump condition.
- Pipe rupture.
- Improper filling, flushing or air removal from pipelines.
- Trapped air inside pipelines.
- Change in power demand of hydraulic turbines

2.3.3 Methods of controlling pressure surges

According to (Douglas et al., 2005) pressure transients problems within pipe systems can be characterized by changes of flow conditions at the system boundaries or by local interactions between transients and local pipe features. The severity of a transient is in general dependent on the rate of change at its source. As for Joukowsky surge, the maximum pressure rise occurs when the flow is brought to rest at an instants closure. In order to protect the system and its components, these transients must be observed, controlled and reduced. The common factor between different surge control devices is that they decrease the rate of change of flow in the system. The following devices or mechanisms are commonly used.

Valve closure control is a mechanism that is used to slow down the final stages of the closure process before the valve slams into its seat. The mechanism can consist of a spring loaded valve which dampens the movement. The absence of closure control can have considerable positive benefits as the rise in pressure can prevent vapor formation and gas release.

An increment in pump inertia increases the time before the pump has stopped and therefore increases rate of change of the transient. This can be achieved by attaching a flywheel to the pump design. A rapid pump stop during power shut down can lead to column separation in turn can lead to low pressure and vapor formation.

Another procedure to protect the system from low pressure column separation zones is to apply air or fluid admission valves which opens at low pressure and allows air or fluid to enter the system and fill up the cavities. This prevents the likeliness of cavity collapse, and hence it prevents pressure surge.

Surge shafts and air vessels can be used for pressure relief during a swift pressure rise in the system. Fluid can be directed to leave the pipe system by entering vertical surge shafts, which can be sealed with gas or air as damper or open to atmospheric pressure.

Relief valves are used to blow off fluid as the pressure rises. It is an uncomplicated and cheap solution. The major drawback is the loss of fluid from the system. However, this can be prevented by connecting a bypass system.

2.4 Computational Fluid Dynamics

A major section of this work will be credited to simulations in ANSYS FLUENT, which provide computational fluid dynamic calculations in practise. It is therefore appropriate to review the theoretical parts of computational fluid dynamics used in this work.

Computational fluid dynamics (CFD) can be described as a junction between mathematics, fluid dynamics and computer science. These three concepts are necessary to make CFD possible. The mathematics is used to describe the physical behavior of fluid dynamics in a way which makes the fluid dynamics quantifiable and countable. Without the possibility of using computers for executing the calculations many real industrial fluid dynamic problems would be extremely time consuming, for not say impossible due to the characteristics of the governing partial differential equations. This section will present the governing equations used in CFD, turbulence theory and important numerical theory regarding convergence in applied CFD.

2.4.1 Governing equations

The dynamics of the fluid is determined by solving the governing equations for conservation of mass, momentum and energy. These equations represent mathematical statements for the conservations of physics which are one of the fundamental cornerstones in CFD.

Conservation of mass

The expression for conservations of mass implements the fundamental rule of physics that matter are unable to be created nor destroyed. In fluid dynamics this can be interpreted as the rate of change of mass within a control volume is equivalent to the mass flux crossing the surface of the volume. This can be expressed according to Eq. 2.34.

$$\frac{d}{dt}\int_V \rho dV = -\int_S \rho V \mathbf{n} dS \tag{2.34}$$

By applying the Gauss's divergence theorem on the surface integral, it can be replaced by a volume integral according to Eq. 2.35.

$$\int_V \left(\frac{\partial \rho}{\partial t} + \nabla(\rho V)\right) dV = 0 \tag{2.35}$$

Equation 2.35 can be applied on any volume of any size. This yields the expression in Eq. 2.36.

$$\frac{\partial \rho}{\partial t} + \nabla(\rho V) = 0 \tag{2.36}$$

Equation 2.36 can be applied on an unsteady three dimensional incompressible flow. This can be expressed with tensor notation index.

$$\frac{\partial u_i}{\partial x_i} = 0 \tag{2.37}$$

Conservation of momentum

The governing equation of momentum balances the forces across a control volume according to Newton's second law of motion. The control volume can experience the influence of body forces and surface forces. These kinds of forces are the only forces that are capable of influencing the rate of change in momentum of the fluid. The body forces consists of gravity, centrifugal, Coriolis, and electromagnetic forces (Tu et al., 2008). The surface forces are caused by the velocity component due to normal stresses and tangential stresses on the surface of the fluid element. The momentum equation is also commonly known as one of the Navier-Stokes equations. This equation is limited to macroscopic conditions, not regarding the movement on a molecular level (Andersson et al., 2012). For a Newtonian fluid the equation of momentum can be expressed as Eq. 2.38.

$$\frac{\partial u_i}{\partial t} + u_j \frac{\partial u_i}{\partial x_j} = -\frac{1}{\rho}\frac{\partial P}{\partial x_i} + \nu \frac{\partial}{\partial x_j}\left(\frac{\partial u_i}{\partial x_j} + \frac{\partial u_j}{\partial x_i}\right) + g_i \tag{2.38}$$

Conservation of energy

The governing equation for conservation of energy is derived from the first law of thermodynamics, which states that energy of an isolated system is constant. The use of the conservation of energy equation is necessary when solving for a compressible flow. However, due to the assumption of isothermal system the energy equation can be neglected. The equation can be expressed as in Eq. 2.39.

$$\frac{dh}{dt} = -\frac{\partial}{\partial x_j}\left[hu_j - k_{eff}\frac{\partial T}{\partial x_j} + \sum m_n h_n D_n \frac{\partial C_n}{\partial x_j} - \tau_{kj}u_k\right] + S_h \tag{2.39}$$

2.4.2 Turbulence

Turbulent flows can be found in most industrial applications, especially in heat exchangers and chemical reactors. The turbulent characteristics such as chaotic motion and randomness are often favorable in the industry to significantly enhance heat- and mass transfer rates. Since turbulence play an important role within industrial fluid mechanics it is important to be able to measure and model turbulent quantities in a proper manner.

Turbulent flows are often studied from an average point of view due to its randomness characteristics. Instant measurements from the same turbulent flow can give different results depending on the time of measurement. This is why turbulence need to be studied on average. In industrial turbulence modeling the use of Reynolds average Navies Stokes equations (RANS) is a common approach to handle turbulent modeling. RANS is based on Reynolds decomposition which is a method where the instantaneous variables are divided into time-averaged and fluctuating quantities (Pope, 2012). Equation 2.40 and 2.41 present velocity and pressure with Reynolds decomposition.

$$u_i = \overline{u_i} + u_i' \tag{2.40}$$

$$p = \overline{p} + p' \tag{2.41}$$

The target of implementing RANS is to handle the Navier-Stokes equations according to Reynolds decomposition. The diffusion in Eq. 2.38 can be rewritten which yields a new version of the momentum equation according to Eq. 2.42.

$$\frac{\partial u_i}{\partial t} + u_j \frac{\partial u_i}{\partial x_j} = -\frac{1}{\rho}\frac{\partial p}{\partial x_i} + \nu \frac{\partial^2 u_i}{\partial x_j \partial x_j} \tag{2.42}$$

The decomposition of the fist term is performed according to the rules of averaging.

$$\overline{\frac{\partial u_i}{\partial t}} = \overline{\frac{\partial}{\partial t}(\overline{u_i} + u_i')} = \overline{\frac{\partial \overline{u_i}}{\partial t}} + \overline{\frac{\partial u_i'}{\partial t}} = \frac{\partial \overline{\overline{u_i}}}{\partial t} + \frac{\partial \overline{u_i'}}{\partial t} = \frac{\partial \overline{u_i}}{\partial t} \tag{2.43}$$

The decomposition of the second term starts by applying the production rule for derivatives.

$$\overline{\frac{\partial u_i u_j}{\partial x_j}} = \overline{u_i}\frac{\partial \overline{u_j}}{\partial x_j} + \overline{u_j}\frac{\partial \overline{u_i}}{\partial x_j} \tag{2.44}$$

This is used to make the decomposition where the neglected term represents the change of y-velocity in y-direction averaged.

$$\frac{\partial \overline{u_i}\,\overline{u_j}}{\partial x_j} = \frac{\partial}{\partial x_j}\left(\overline{\overline{u_i}\,\overline{u_j}} + \overline{u_i' u_j'}\right) =$$

$$= \frac{\partial}{\partial x_j}\left(\overline{u_i}\,\overline{u_j}\right) + \frac{\partial}{\partial x_j}\left(\overline{u_i' u_j'}\right) + \cancel{\overline{u_i}\frac{\partial \overline{u_j}}{\partial x_j}} + \overline{u_j}\frac{\partial \overline{u_i}}{\partial x_j} + \frac{\partial}{\partial x_j}(\overline{u_i' u_j'}) = \overline{u_j}\frac{\partial \overline{u_i}}{\partial x_j} + \frac{\partial}{\partial x_j}(\overline{u_i' u_j'}) \tag{2.45}$$

This is used to complete the final expression.

$$\frac{\partial \overline{u_i}}{\partial t} + \overline{u_j}\frac{\partial \overline{u_i}}{\partial x_j} = -\frac{1}{\rho}\frac{\partial \overline{p}}{\partial x_i} + \nu\frac{\partial^2 \overline{u_i}}{\partial x_j \partial x_j} - \frac{\partial}{\partial x_j}\left(\overline{u_i' u_j'}\right) \tag{2.46}$$

This is the general form of the momentum equation for a incompressible Newtonian fluid. Viscous stresses, isentropic stresses from the mean pressure field and the apparent stress arising from the fluctuating velocity field are all represented in Eq. 2.46. The term $-\rho\overline{u_i' u_j'}$ arises from the fluctuating velocity field and is conventionally referred as the Reynolds stress (Pope, 2012). The use of Reynolds average Navies-Stokes equations introduces a set of equations which contains more unknowns than available equations. In addition to the three velocity components and the mean pressure field, the Reynolds stresses needs to be determined to solve the equations, which introduces the closure problem which needs to be handled in order to solve Eq. 2.46. A known procedure is to use Boussinesq's hypothesis.

The stress-rate-of-strain for a Newtonian fluid can be expressed according to Eq. 2.47.

$$\tau_{ij} = -p\delta_{ij} + \mu\left(\frac{\partial u_i}{\partial x_j} + \frac{\partial u_j}{\partial x_i}\right) \tag{2.47}$$

The turbulent-viscosity hypothesis, also called Boussinesq's hypothesis is mathematically in analogy with the stress-rate-of-strain for a Newtonian fluid. Boussinesq's hypothesis states that the deviatoric Reynolds stress tensor is proportional to the mean rate of strain according to Eq. 2.48.

$$-\rho\overline{u_i' u_j'} = \rho\nu_T\left(\frac{\partial \overline{u_i}}{\partial x_j} + \frac{\partial u_j}{\partial x_i}\right) - \frac{2}{3}\rho k\delta_{ij} = 2\rho\nu_T\overline{S_{ij}} - \frac{2}{3}\rho k\delta_{ij} \tag{2.48}$$

By combining Eq. 2.48 and Eq. 2.46 through insertion, the equations of motion can now be written as Eq. 2.49.

$$\frac{\partial \overline{u_i}}{\partial t} + \overline{u_j}\frac{\partial \overline{u_i}}{\partial x_j} = -\frac{1}{\rho}\frac{\partial \overline{p}}{\partial x_i} - \frac{2}{3}\frac{\partial k}{\partial x_i} + \frac{\partial}{\partial x_j}\left[(\nu + \nu_T)\left(\frac{\partial \overline{u_i}}{\partial x_j} + \frac{\partial \overline{u_j}}{\partial x_i}\right)\right] \tag{2.49}$$

Turbulence models

There is a variety of different available turbulence models which can be used during CFD-simulations. Certain models are developed and specialized for certain flow problems, for example the one equation Spalart-Allmaras model which is developed for aerodynamic applications where a single model equation for turbulent viscosity ν_T is solved (Pope, 2012). Only two-equations models will be used in this work due to the complex flow characteristics.

Standard k-ϵ model

One of the most common turbulence models in the industry is the $k-\epsilon$ model, which is a two equation model where transport equations are solved for turbulent kinetic energy k and dissipation of turbulent kinetic energy ϵ. The Standard $k-\epsilon$ model is derived by applying Reynolds decomposition on the equation for kinetic energy, assuming that the flow is fully turbulent and neglecting molecular viscosity. This yields a turbulence model which is only valid for fully turbulent flows according to the FLUENT v16 manual. The modeling of the turbulent kinetic energy k is described in Eq. 2.50.

$$\underbrace{\frac{\partial k}{\partial t}}_{\text{I}} + \underbrace{\overline{u_j}\frac{\partial k}{\partial x_j}}_{\text{II}} = \underbrace{-\overline{u_i u_j}\frac{\partial \overline{u_i}}{\partial x_j}}_{\text{III}} - \underbrace{\nu\overline{\frac{\partial u_i}{\partial x_j}\frac{\partial u_i}{\partial x_j}}}_{\text{IV}} + \frac{\partial}{\partial x_j}\left(\underbrace{\nu\frac{\partial k}{\partial x_j}}_{\text{V}} - \underbrace{\frac{\overline{u_i u_i u_j}}{2}}_{\text{VI}} - \underbrace{\frac{\overline{u_j p}}{\rho}}_{\text{VII}}\right) \tag{2.50}$$

The representation of the of the terms in Eq. 2.50 are described in the follwing list.

I. Accumulation of k.

II. Convection of k by the mean velocity.

III. Production of k, large eddies extract energy from the mean flow.

IV. Dissipation of k by viscous stress, whereby turbulent kinetic energy is transformed into heat.

V. Molecular diffusion of k.

VI. Turbulent transport by velocity fluctuations.

VII. Turbulent transport by pressure fluctuations.

The terms III, IV and VII must be approximated with some correlation in order to enable closure for the production, dissipation and diffusion term. Hence, the Boussinesque approximation in Eq. 2.48 is applied which yields the expression described in Eq. 2.51 for the production of turbulent kinetic energy.

$$-\overline{u_i u_j}\frac{\partial \overline{u_i}}{\partial x_j} = \nu_T \left(\frac{\partial \overline{u_i}}{\partial x_j} + \frac{\partial \overline{u_j}}{\partial x_j}\right)\frac{\partial \overline{u_i}}{\partial x_j} - \frac{2}{3}k\frac{\partial \overline{u_i}}{\partial x_i} \tag{2.51}$$

The dissipation of turbulent kinetic energy is defined according to Eq. 2.52.

$$\epsilon = \nu \left(\overline{\frac{\partial u_i}{\partial x_j}\frac{\partial u_i}{\partial x_j}}\right) \tag{2.52}$$

The final closure is required to describe the turbulent transport of k. The terms VI and VII are normally modelled with the assumption of a gradient-diffusion transport mechanism (Andersson et al., 2012), which allows the turbulent transport due to velocity and pressure fluctuations be modeled as Eq. 2.53.

$$-\frac{\overline{u_i u_i u_j}}{2} - \frac{\overline{u_j p}}{\rho} = \frac{\nu_T}{\sigma_k}\frac{\partial k}{\partial x_j} \tag{2.53}$$

Here σ_k is the Prandtl-Schmidt number and ν_T is the turbulent viscosity. These closure modifications yield the final expression for the modeling of k in the Standard k-ϵ model.

$$\frac{\partial k}{\partial t} + \overline{u_j}\frac{\partial k}{\partial x_j} = \nu_T \left[\left(\frac{\partial \overline{u_i}}{\partial x_j} + \frac{\partial \overline{u_j}}{\partial x_j}\right)\frac{\partial \overline{u_i}}{\partial x_j}\right] - \epsilon + \frac{\partial}{\partial x_j}\left[\left(\nu + \frac{\nu_T}{\sigma_k}\right)\frac{\partial k}{\partial x_j}\right] \tag{2.54}$$

To finally close Eq. 2.54 the dissipation of turbulent kinetic enery ϵ and turbulent viscosity ν_T need to be calculated. Since the turbulence model is a two-equation model, ϵ is modelled with a second transport equation. A general expression for the dissipation of turbulent kinetic energy ϵ can be expressed as Eq. 2.55.

$$\underbrace{\frac{\partial \epsilon}{\partial t}}_{\text{I}} + \underbrace{\overline{u_j}\frac{\partial \epsilon}{\partial x_j}}_{\text{II}} = \underbrace{C_{\epsilon 1}\nu_T \frac{\epsilon}{k}\left[\left(\frac{\partial \overline{u_i}}{\partial x_j} + \frac{\partial \overline{u_j}}{\partial x_j}\right)\frac{\partial \overline{u_i}}{\partial x_j}\right]}_{\text{III}} - \underbrace{C_{\epsilon 2}\frac{\epsilon^2}{k}}_{\text{IV}} + \underbrace{\frac{\partial}{\partial x_j}\left[\left(\nu + \frac{\nu_T}{\sigma_\epsilon}\right)\frac{\partial \epsilon}{\partial x_j}\right]}_{\text{V}} \tag{2.55}$$

The representation of the of the terms in Eq. 2.55 are described in the follwing list.

I. Accumulation of ϵ.

II. Convection of ϵ by the mean velocity.

III. Production of ϵ.

IV. Dissipation of ϵ.

V. Diffusion of ϵ.

The turbulent viscosity ν_T is modeled in order to close the system of equations. It is modeled using a coefficient C_μ, the turbulent kinetic energy k and the dissipation of turbulent kinetic energy ϵ according to Eq. 2.56.

$$\nu_T = C_\mu \frac{k^2}{\epsilon} \tag{2.56}$$

The system of equations contain a number of universal closure coefficient which can be assumed to be constant. However, they can vary slightly from one flow to another (Andersson et al., 2012). The settings of the constant coefficients used in this thesis will be the default values in FLUENT and will be unchanged during all simulations. It is assumed that the default settings will be suitable for the flow cases used in this thesis. The coefficients and their corresponding values for the Standard k-ϵ model are presented in the Tab. 2.1.

Table 2.1: Closure coefficients used in the k-ϵ model

Coefficient	**Value [-]**
C_μ	0.09
$C_{\epsilon 1}$	1.44
$C_{\epsilon 1}$	1.92
σ_k	1.00
σ_ϵ	1.30

Realizable k-ϵ model

There are two main difference between the Realizable k-ϵ model and the Standard k-ϵ model. First, the Realizable k-ϵ model uses another formulation of the coefficient C_μ in Eq. 2.56 according to Eq. 2.57.

$$C_\mu = \frac{1}{A_0 + A_S \frac{kU^*}{\epsilon}} \tag{2.57}$$

Here, C_μ is a function of mean strain and rotation rates, angular velocity of the system rotation and the turbulence fields of k and ϵ according to the FLUENT v16 manual. The second difference is the use of a modified transport equation for the dissipation rate of turbulent kinetic energy ϵ. This equation has been derived from an exact equation for the transport of mean-square vorticity fluctuation.

The Realizable k-ϵ model provides suitable performance for flows involving rotation, boundary separation with strong adverse pressure gradients. These properties should be beneficial as the opening angle of the valve decreases and the flow path is hampered. According to (Davis et al., 2012) the Realizable k-ϵ model should show a superior ability to reach a stable solution of mean flow with complex geometries.

SST k-ω model

The SST k-ω turbulence model is a common two-equations turbulence model used in the industry. SST is an abbreviation for shear stress transport which combines the useful properties of both k-ϵ and k-ω models. The use of k-ω formulations for the inner parts at the boundary layer which makes the model useful through the viscous sublayer at the walls. The sensitivity of inlet free-stream turbulence properties of the k-ω-model is avoided by switching to k-ϵ at the free-stream. The two equations for turbulent kinetic energy and ω is expressed in Eq. 2.58 and Eq. 2.59.

$$\frac{\partial k}{\partial t} = \overline{u_j}\frac{\partial k}{\partial x_j} = \nu_T \left[\left(\frac{\partial \overline{u_i}}{\partial x_j} + \frac{\partial \overline{u_j}}{\partial x_i} \right) \frac{\partial \overline{u_i}}{\partial x_j} \right] - \beta k\omega + \frac{\partial}{\partial x_j} \left[\left(\nu + \frac{\nu_T}{\sigma_k} \right) \frac{\partial k}{\partial x_j} \right] \tag{2.58}$$

$$\frac{\partial \omega}{\partial t} = \overline{u_j}\frac{\partial \omega}{\partial x_j} = \alpha \frac{\omega}{k} \nu_T \left[\left(\frac{\partial \overline{u_i}}{\partial x_j} + \frac{\partial \overline{u_j}}{\partial x_i} \right) \frac{\partial \overline{u_i}}{\partial x_j} \right] - \beta \omega^2 + \frac{\partial}{\partial x_j} \left[\left(\nu + \frac{\nu_T}{\sigma_k} \right) \frac{\partial \omega}{\partial x_j} \right] \tag{2.59}$$

The coefficients used to close the equations are presented in Tab. 2.2.

Table 2.2: Closure coefficients used in the k-ω model

Coefficient	**Value [-]**
C_{α_1}	0.52
C_{β_1}	0.072
C_{β^*}	0.09
σ_k	2.00
σ_ω	2.00

Wall treatment

Close to the boundary walls the calculation of the turbulent flow is impeded and is in need of modifications to the basic turbulence models. Handling the flow close to the walls is performed by using wall-functions which defines boundary conditions at a distance from the wall. The turbulence equations are not solved in the region between the wall and where the boundary layer applies (Pope, 2012).

Standard Wall Functions

The Standard wall functions are wall functions available in FLUENT based on the law of the wall. The foundation of these models is the presence of an inner layer at which the mean velocity profile is determined by viscous scales, independent of the boundary layer thickness and mean center line velocity (Pope, 2012). The mean velocity is modeled according to the law of the wall which can be expressed by Eq. 2.60.

$$U^* = \frac{1}{\kappa} ln(Ey^*) \tag{2.60}$$

Here U^* is the dimensionless velocity, κ is the von Kármán constant and E is an empirical constant. U^* is defined according to Eq. 2.61.

$$U^* \equiv \frac{U_p C_\mu^{1/4} k_p^{1/2}}{\tau_w/\rho} \tag{2.61}$$

Here U_p is the mean velocity of the fluid at the wall-adjacent cell centroid, C_μ is a constant affecting the turbulent viscosity, k_p is the turbulent kinetic energy at the wall-adjacent cell centroid and τ_w is the wall shear stress. y^* is the dimensionless distance from the wall and is defined according to Eq. 2.62.

$$y^* \equiv \frac{\rho C_\mu^{1/4} k_p^{1/2} y_p}{\mu} \tag{2.62}$$

The magnitude of y^* is of importance regarding the accuracy of the solution and is dependent on the overall Reynolds number of the flow. According to the FLUENT v16 manual, it is more important to ensure that the boundary layer is covered with a sufficient number of inflation cells than to ensure a certain y^*-value.

Scalable Wall Functions

Scalable Wall Functions is used to force the usage of the log law, which differs from the Standard Wall Functions. This is achieved by setting a limiter in the y^* calculations according to Eq. 2.63.

$$\widetilde{y^*} = MAX(y^*, y^*_{limit}) \tag{2.63}$$

Scalable wall functions does not deteriorate as Standard wall functions under grid refinement with y^+ below 15. These wall functions produce consistent results for grids of arbitrary refinement. For grids that are coarser, the Standard- and Scalable wall functions are identical.

Enhanced Wall Functions

Enhanced wall treatment is a near-wall modeling method that combines a two-layer model with enhanced wall functions in order to resolve the boundary layer down to the viscous sublayer. When the near-wall mesh is fine enough to be able to resolve the viscous sublayer (approximately $y^+ \approx 1$), then the Enhanced

wall treatment will be equal to the traditional two-layer zonal model. However, the restriction regarding the near-wall mesh must be sufficiently fine everywhere which can result in an extensive computational requirement. Ideally, it is preferable to have a near-wall formulation that can be used with both coarse meshes, also called wall-function meshes, as well as fine meshes with low-Reynolds-number meshes. In addition, the excessive error should not have to be taken into consideration for intermediate meshes that are too fine for the near-wall cell centroid to lie in the fully turbulent region and also too coarse to properly resolve the sublayer according to the FLUENT v16 manual.

2.4.3 Discretization schemes

Discretization implies on transferring continuous equations into discrete counterparts that can be handled by a computer. During CFD-simulations the governing equations and additional transport equations are discretized according to different schemes optional to the user. These schemes are derived using Taylor series on the partial differential equations. The implementation of the Taylor series determines the accuracy in time, spatial accuracy and which computational nodes that are to be used.

This work will use the second order upwind discretization scheme when solving the continuity equation and momentum equation. The first order upwind discretization scheme will be used when solving turbulence properties.

2.4.4 Convergence

Convergence is an important criteria when solving partial differential equations and should be considered when a numerical method is used. However, the quantification and measurement of convergence is not straight forward which is why aspects like consistency and stability conditions is used when judging convergence of a numerical method. The aspect of consistency is of importance when using discretized schemes of partial differential equations. A numerical method can be considered consistent as the error between the discretized equations and the exact equations approaches zero when time step, Δt, and spatial spacing, Δx, Δy, Δz, goes towards zero. For most discretization schemes the error is proportional to the nth order of the scheme. Stability occurs when spontaneous perturbations in the solution to the system of algebraic equations decay

When solving a system of algebraic equations using CFD, the equations are often solved iteratively. There are three major aspects that affects the rate of iterative convergence (Tu et al., 2008). First, the discretized equations for continuity, momentum, energy etc. have to reach a specified convergence criterion which usually is a tolerance level for every nodal location. This convergence criterion often uses residuals as an indicator on weather a solution tend to converge or diverge. Secondly, the numerical solution is unchanged after additional iterations. Lastly, mass, momentum, energy and scalar balances have been achieved.

Residuals can be considered the imbalances of the discretized governing equation. For any given local transport variable ϕ at a cell P, the discretized partial differential equation can be written as seen in Eq. 2.64.

$$a_p \phi_p = \sum a_{nb} \phi_{nb} + b_p \tag{2.64}$$

Here a_p is the central coefficient and a_{np} neighbouring coefficients. b_p is the contribution of the constant part of the source term S_c in $S = S_C + S_P \phi$ and of the boundary conditions. These coefficients are continuously updated during the iterative process. Equation 2.64 is not valid in the beginning of the iteration process which introduces the imbalance factor R_p (Tu et al., 2008).

$$R_P = \sum a_{nb} \phi_{nb} + b_p - a_p \phi_p \tag{2.65}$$

This is often applied for all nodal points, creating a global unscaled residual according to the expression in Eq. 2.66.

$$R = \sum |R_p| \tag{2.66}$$

This global residual is used together with the convergence tolerance which can be defined by the user according to Eq. 2.67.

$$R \leq \epsilon \tag{2.67}$$

Here ϵ is the convergence tolerance. The choice of convergence tolerance can have a great impact in both solution results and computational time which has to taken under consideration with respect to computational performance and accuracy. Monitored residuals are often scaled to facilitate the judging of convergence, which is often enabled during the simulation set-up in the CFD-software. There is no universal approach to judge convergence suitable for every CFD-case. It is often useful to combine monitored residuals with monitored quantities of interest depending on the kind of problem, for example drag and lift force for aerodynamic problems and heat transfer coefficient for temperature dependent problems.

2.5 One-dimensional codes

Even though many industrial fluid dynamic problems are three dimensional, it can be applicable to derive one-dimensional models based on suitable theory and experiments. The incitement is to develop fast running general models to calculate quantities of interest. This work will use results from CFD-simulations in order to investigate how a one dimensional swing check valve model can be implemented according to the theory of (Li and Liou, 2003).

There are a number of commercial one dimensional codes where each code uses a different swing check valve model and approach to calculate the loss. Three of these codes will be reviewed in order to demonstrate similarities and differences in calculation methods. In addition to RELAP5, the one-dimensional codes DRAKO and DYVRO mod. 3 will be reviewed.

2.5.1 RELAP5

The development of RELAP5 started in the early 1980's at the Idaho Natinal Engineering Laboratory (INEL) for the U.S. Nuclear Refulatory Comission (NRC). It is one of the most common codes for transient flow simulations within the nuclear industry, especially in Sweden. The code includes generic components which are widely found in nuclear power plant systems, e.g. pumps, valves, pipes and turbines. The code also provide special process models to model effects in these system, e.g. choked flow and abrupt area change models. Regarding swing check valves, the built in valve model is occasionally not considered to give sufficiently realistic results. This is mainly due to the characteristics of the swing check valve, where the closure process can be considered a fast transient. RELAP5 does on the other hand not focus on a specific component, rather a system of transients.

The swing check valve component in RELAP5 is called inertial check valve (*inrvlv*) and its motion is governed by Newton's second law of motion according to Eq. 2.5. The specific equation of motion can be expressed according to Eq. 2.68.

$$T_{DP} + T_F + T_w = I\ddot{\theta} \tag{2.68}$$

The torque component T_{DP} is the hydraulic torque caused by the pressure difference across the valve. T_{DP} is calculated according to Eq. 2.69.

$$T_{DP} = (P_K - P_L)A_P L \tag{2.69}$$

Here P_K and P_L are the pressures in the hydraulic cell just upstream respectively downstream of the valve component. The pressure difference is used with the projected area of the valve disc A_P and the length of the lever arm L. The loss coefficient is calculated according to pressure loss due to an orifice. The orifice geometry is presented in Fig. 2.6 and is used to define a number of area ratios.

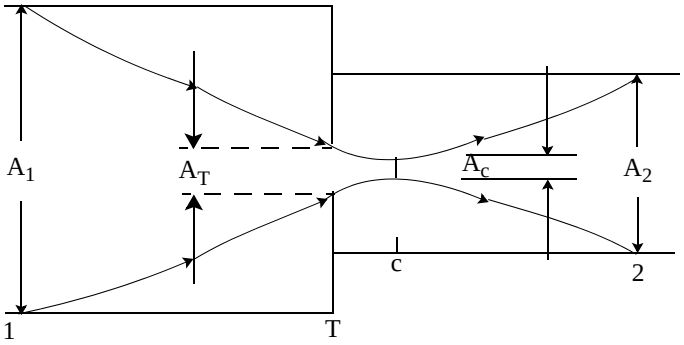

Figure 2.6: Areas used in the pressure loss model (The RELAP5-3D© Code Development Team, 2005).

$$\epsilon_c = \frac{A_C}{A_T} \quad \epsilon_T = \frac{A_T}{A_1} \quad \epsilon = \frac{A_2}{A_1}$$

Here, ϵ_c is the area contraction ratio at the vena-contracta relative to the minimum physical area. ϵ_T is the ratio of the minimum physical area to the upstream flow area. ϵ is the ratio of the downstream and upstream area. According to (Turesson, 2011) the throat area A_T is assumed to be calculated according to Eq. 2.70.

$$A_T = \frac{min(A_1|A_2)}{A_{junction}}(1 - cos(\theta))C_c \tag{2.70}$$

The contraction coefficient C_c is proportional to the fraction of opening area $1 - cos(\theta)$. The torque due to Coulomb friction T_F is dependent on the vena-contracta area which depends the minimum pressure difference across the valve required to initiate motion, also called the cracking pressure.

$$T_F = \Delta P_f A_R L \tag{2.71}$$

Here, A_R is the area of the disc and L is the leverarm between the hinge pin and center of gravity. The dynamic pressure loss associated with the expansion from the vena-contracta to the downstream section is given by Eq. 2.72.

$$\Delta P_f = \frac{1}{2}\rho\left(1 - \frac{A_c}{A_2}\right)^2 v_c^2 \tag{2.72}$$

2.5.2 DRAKO

DRAKO is a german abbreviation for Druckwellenberechnung in Rohrleitungssystemen mit allgemeinen Komponenten, translated in English to pressure wave calculation in piping systems with common components. The software is used to calculate unsteady flow phenomena in complex piping systems. It includes an extensive collection of boundary elements with which practically any pipeline system with valves, non-return valves, vessels, diaphragms, air chambers, junctions, fittings, containers, pumps, etc. can be modeled. DRAKO is a three-equation program that calculates one-dimensional flows. Any liquids, two-phase mixtures, steams or gasses can be handled as a medium with the program (KAE, 2005).

The equation of motion used in DRAKO consists of hydraulic torque, torque due to bearing friction and weight. It is expressed according to Eq. 2.73.

$$T_{hyd} + T_F + T_w = I\ddot{\theta} \tag{2.73}$$

The hydrodynamic torque is calculated according to Eq. 2.74 where both a static and a dynamic component is included. The dynamic component handles the diversion of flow using the relative velocity between flow and valve.

$$T_{hyd} = (p_K - p_L)A_{disc}L + |v_{rel}|v_{rel}\rho A_{seat}cos^2(\theta)L \tag{2.74}$$

The term expressing the relative velocity v_{rel} is calculated according to Eq. 2.75, where U_1 and A_1 are the velocity and area at the upstream pipe.

$$v_{rel} = \frac{U_1 A_1}{A_{seat}} - L\omega cos(\theta) \tag{2.75}$$

The torque due to weight is calculated according to Eq. 2.76 where

$$T_w = \left(1 - \frac{\rho_2}{\rho_{st}}\right) mgsin(h + Hg)L_{cg} \tag{2.76}$$

2.5.3 DYVRO mod. 3

The calculation software DYVRO mod. 3 is a commercial code used to investigate unsteady flow processes in branched piping systems. The code contains pre defined models for both a tilting disc valve and a swing check valve. These valve models are based on Eq. 2.5 to capture the motion of the valve as detailed as possible (DYVRO, 2012). The total torque component used in DYVRO can summarized by the individual torque components according to Eq. 2.77.

$$T_{tot} = T_{pressure} + T_{impuls} + T_{weight} + T_{buoyancy} + T_{damping} + T_{damping,additional} \tag{2.77}$$

The torque due to differential pressure $T_{pressure}$ across the valve disc is calculated with the pressure difference across the valve disc, the disc area and the projected lever arm between the hinge pin and the disc center according to Eq. 2.78.

$$T_{pressure} = \Delta p A_{disc} cos\theta L \tag{2.78}$$

This torque only handles static pressure effects which introduces the need of a dynamic torque component which takes the relative velocity between the moving valve disc and fluid flow into consideration. This torque components is called T_{impuls} and is modeled according to Eq. 2.79.

$$T_{impuls} = \rho(v_{fluid} - \dot{\theta}L)|v_{fluid} - \dot{\theta}L|A_{disc}cos\theta L \tag{2.79}$$

The use of absolute value takes the direction of through flow into account. The torque due to weight and the torque due to the displacement of fluid is divided into two torque components, T_{weight} and $T_{buoyancy}$.

$$T_{weight} = m_{disc}gsin\theta L \tag{2.80}$$

$$T_{buoyancy} = m_{fluid}gsin\theta L \tag{2.81}$$

DYVRO uses a damping friction torque based on the theory of (Pandula and Halász, 2002) which treats a rotational disc in viscous medium with respect to the influences of eccentricity, according to Eq. 2.82.

$$T_{damping} = \left[\frac{D_{disc}^5}{60} + \frac{D_{disc}^3}{2}L^2\right] \rho\dot{\theta}|\dot{\theta}| \tag{2.82}$$

It is possible to add a second damping torque to the equation of motion to tune the valve behaviour. This torque components is defined as seen in Eq. 2.83.

$$T_{damping,additional} = 6kb_{krit}I_{tot}\dot{\theta} \tag{2.83}$$

Here b_{krit} is the critical damping coefficient and k is a constant which has been validated to have the value of $k = 0.2$ for best results. The critical damping coefficient is defined as seen in Eq. 2.84.

$$b_{krit} = \sqrt{\frac{Lg(m_{disc} - m_{fluid})}{I_{tot}}} \tag{2.84}$$

3 Method

To be able to retrieve reliable data in order to derive and use correlations for one-dimensional code implementation, results must be extracted through CFD-simulations. To ensure the reliability in results from CFD-simulations, numerous changes in simulation properties will be examined to make a thorough sensitivity analysis. This analysis will examine the effects of mesh structure and simulation options in FLUENT.

3.1 Geometry

The geometry of the swing check valve used in this work has previously been created by TÜV NORD from drawings of the valve Staal40 AKKS DN400 PN40 from the manufacturer KSB. The geometry used in FLUENT consists of two pipe parts and one valve part. The initial geometry was created in GAMBIT and is modified in ANSYS DesignModeler in order to facilitate the meshing procedure. The upstream pipe is connected to the valve where the flow encounter a 90 degrees expansion as it passes the valve seat and enters the valve housing. The valve disc is connected to a hinge pin at the center of rotation. The maximum range of rotation stretches from 2.51 degrees to 60 degrees relative to a completely vertical position. Geometric valve data is presented in Table 3.1 and used in Fig. 3.1.

Table 3.1: Geometric valve data

Parameter	**Value**	**[unit]**
Lever arm, L_{arm}	266.3	[mm]
Radius to center of gravity, L_{cg}	247.3	[mm]
Minimal valve angle, θ_{min}	2.51	[°]
Maximal valve ange, θ_{max}	60	[°]
Diameter of disc, D_{disc}	420.0	[mm]
Inner diameter of pipe, D_{pipe}	378.0	[mm]
Moved mass of disc, m	46.66	[kg]
Moment of inertia, I_z	3.863	[kgm^2]
Disc area, A_{disc}	0.1385	[m^2]
Seat area, A_s	0.1122	[m^2]

The available model has been simplified compared to the original drawings in several means which prevents some studies in result comparison. The lever arm has been cut off from the hinge pin in a similar approach as in the work of (Boqvist, 2013) Since both pipes and valve are symmetric in the xy-plane, the whole geometry has been cut in half using a symmetry plane along the xy-plane. An apparent result of this approach is that the amount of computational cells will be heavily reduced. This approach should not have any major impacts on the results as long as the used turbulence model is based on RANS. However, this will be investigated. An overview illustration of the model can be seen in Fig. 3.2.

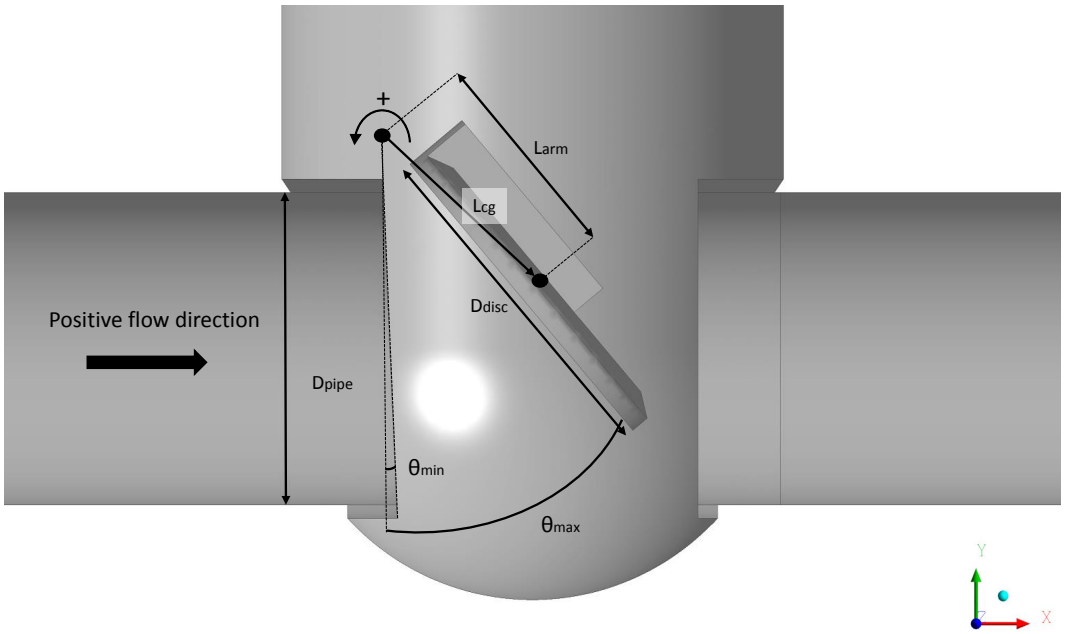

Figure 3.1: Schematic illustration of the valve in the xy-plane. The circular arrow indicates counter-clockwise as positive rotational direction

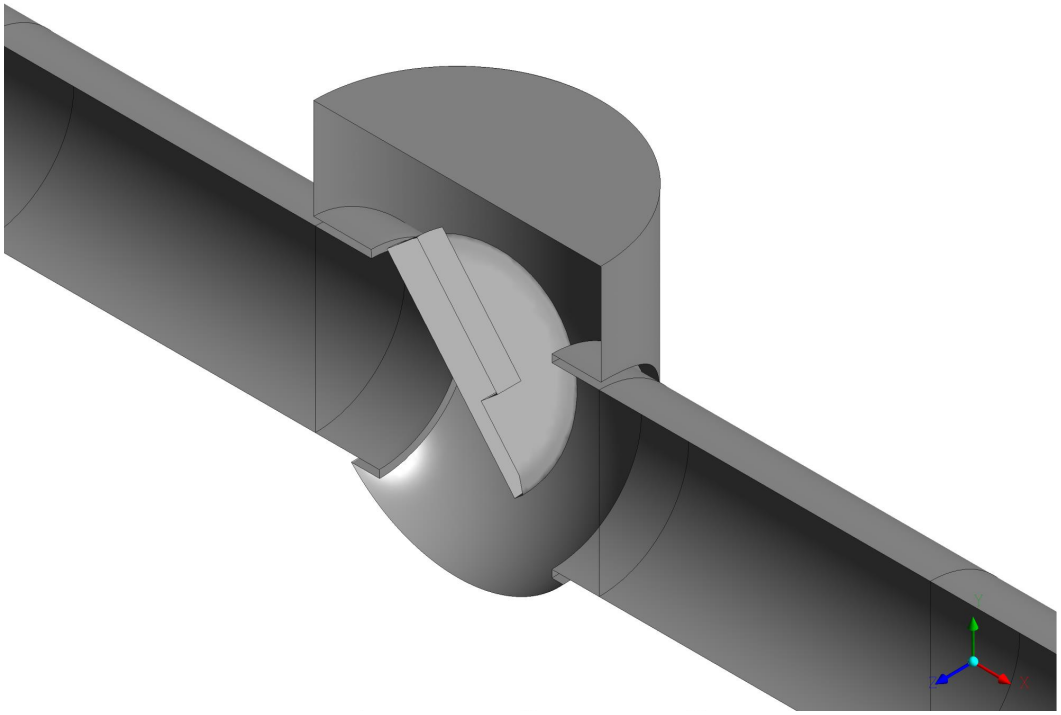

Figure 3.2: Three-dimensional overview of the valve model. The symmetry plane has been removed for a clear view inside the valve.

It is assumed that the torque caused by friction at the hinge pin is negligible compared to hydraulic- and weight torque. In the work of (Li and Liou, 2003) it is stated that this frictional torque will have less impact on larger valves, which the Staal40 AKKS DN400 PN40 is compared to the valve used by the authors. In the work by (Boqvist, 2013) it is demonstrated that partly removal of the rod during simulation has an negligible effect on the results.

3.2 Mesh

The model has originally been meshed in GAMBIT and is redefined in ANSYS Meshing. The mesh is a hybrid mesh where the pipe segments has structured mesh and the valve housing has unstructured mesh. It it important to handle the boundary flow in terms of convergence. However, near wall flow in the pipes is assumed not to have any important effect of the movement of the valve disc and have therefore not been resolved with a particularly fine mesh, however, some precautions has been made in order to set a suitable first layer cell height, see section 3.6. This saves computational time without loss of important information regarding the movement. The mesh used in the sationary simulations is illustrated in Fig. 3.3 where the opening angle is 40 degrees.

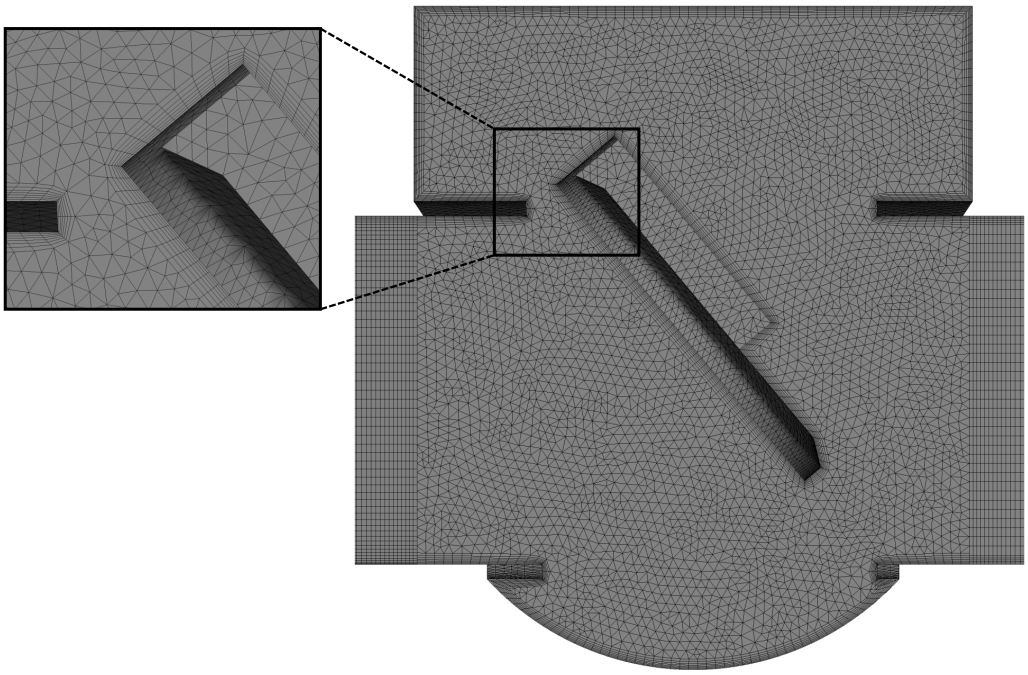

Figure 3.3: Mesh structure at the symmetry plane for the valve house, valve disc and pipes. The zoomed box show the inflation layer at the valve disc and upper region of the seat.

The mesh used in the transient cases has been created with the movement of the valve disc taken into consideration. The boundary layer mesh consists of a number of prismatic layer cells to resolve boundary flow with reasonable accuracy. The optimization of prismatic layers around the valve disc has been compromised in order to be able to close the valve as much as possible. It is of great importance to reach as low opening angle as possible in order to capture potential pressure increases due to Joukowsky surge. The valve will not be able to fully close since there must be at least one compressed cell layer between the valve disc and the seat. The comparison between the compromised prismatic inflation layer on the valve disc and the inflation layer on valve disc used in the stationary simulations can be seen in Fig. 3.4.

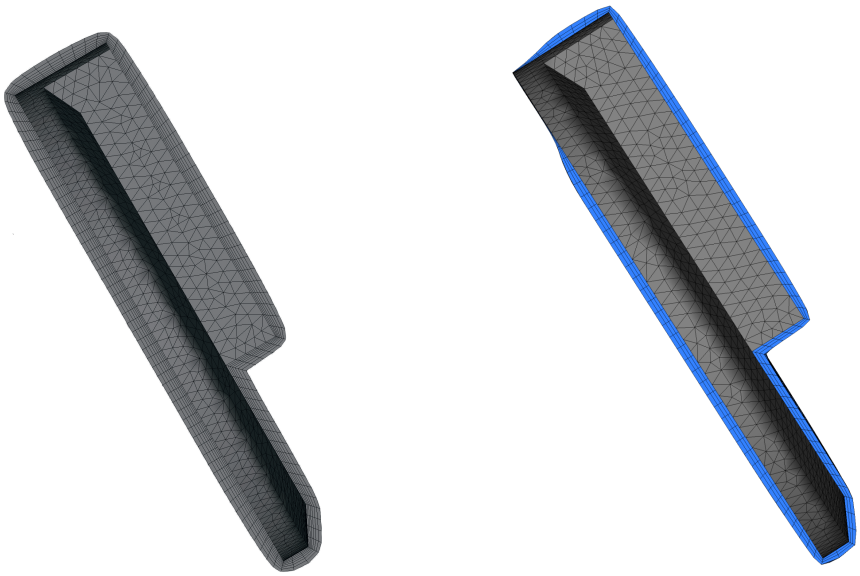

(a) Stationary cases. (b) Transient cases.

Figure 3.4: Mesh in the symmetry plane for the prismatic inflation layers used in the stationary and transient simulations.

The main difference between the mesh used in the stationary cases is the prismatic layers around the valve disc and at the seat of tfhe valve. Since the valve will not hit the seat during stationary simulations, the cells of the prismatic layers has been allowed to be less skeweded. The mesh used in the stationary cases is examined with different magnitudes of cell density in order to reach an acceptable level of mesh independence. The change in stationary torque coefficient C_{HS} and computational time will be taken into consideration when determining the final mesh. The mesh used in the transient cases will undergo a similar mesh independence investigation, however, due to computational performance, the cell density will be lower than for the stationary cases. Since the transient simulations involve moving mesh zones it is suitable to use equally sized tetrahedral cells in the valve domain according to ANSYS Support.

3.2.1 Dynamic mesh settings

The symmetry plane of the model complicates the dynamic zone set up compared to a full body model. The main difference is that remeshing is not only necessary in the bulk mesh, it it also essential to allow the cells on the surface of the symmetry plane to remesh. The remeshing of the bulk cells is handled by the option *Local Cell* in FLUENT. The local cell remeshing method allows FLUENT to mark cells based on skewness and defined length scales provided by the user. Cells are restructured when their geometry exceeds the skewness and/or the length scale limits. Since the cells on the symmetry plane are face cells, the remeshing of the cells on the symmetry plane will be controlled by the option *Face Region*. The face region option allows cells adjacent to a deforming surface to remesh depending on the specified maximum or minimum length scale. It would also be possible to remesh the face cells according to the option *Local Face* method, where the cells are remeshed based on skewness It is important to separate and create a new zone of the prismatic layer closest to the valve disc wall in order to allow the *Face Region* method to make a proper remeshing. This zone should cope with the motion of the valve disc by setting the SDOF-motion to passive. The zone separation automatically creates an interior surface between the valve disc wall and first prismatic layer. This surface is also allowed to passively cope the SDOF-motion of the valve disc.

The motion of the valve disc is controlled by an UDF which is customized to work with the SDOF-solver. The solver computes the external forces and torques due to the flow on the selected dynamic zones. In this work, the SDOF-solver is applied on the valve disc wall. The surrounding prismatic layer is set to cope with the valve disc motion, the SDOF-solver will not perform any calculation on that surface. The symmetry plane and the fluid zone of the valve is set as a deforming zones in order to activate the remeshing and smoothing options. The deformation of the bulk mesh is controlled by the spring-based smoothing- and remeshing function. The spring-based smoothing function allows the cells to stretch and

contract according to Hooke's law applied on a network of springs, where the spring constant is set by the user. A displacement at a given boundary node will generate a force proportional to the displacement along all the springs connected to the node. Using Hook's law, the force on a mesh node can be calculated according to Eq. 3.1.

$$\overrightarrow{F_i} = \sum_{n_j}^{n_i} k_{ij}(\Delta\overrightarrow{x_j} - \Delta\overrightarrow{x_i}) \tag{3.1}$$

The node displacements of node i and the neighbouring node j is expressed with $\Delta\overrightarrow{x_i}$ and $\Delta\overrightarrow{x_j}$. The number n_i is the number of connected nodes to node i. The spring constant k_{ij} determines the stiffness of the system. Alternatively the smoothing operation can also be based on diffusion, where the mesh motion is controlled by the diffusion equation 3.2.

$$\nabla(\gamma\nabla\overrightarrow{u}) = 0 \tag{3.2}$$

Equation 3.2 is also called the Laplace equation and it describes how the prescribed boundary motion diffuses into the interior of the deforming mesh. The boundary conditions for Eq. 3.2 is either provided by the user through UDF-functions or by the computed SDOF boundary motion. A diffusion coefficient is set by the user where a constant coefficient results in a uniformly diffusion throughout the interior mesh and a nonuniform coefficient results in less relative motion between moving boundaries and the interior.

To allow the mesh to update within a time step the implicit mesh update is enabled. This approach is beneficial to enhance the coupling between the converging flow results and the motion of the mesh, resulting in a more robust sequence of calculations. By updating the mesh within a time step the time step size can be larger than without the implicit update method.

3.3 User Defined Functions

User defined functions (UDF) are user written C-functions which can dynamically be implemented into ANSYS FLUENT to enhance the standard features of the software. Three different UDF:s have been used in this work which contain the following macros.

- *DEFINE_SDOF_PROPERTIES*
- *DEFINE_EXECUTE_AT_END*
- *DEFINE_PROFILE*

The UDF which uses the macro *DEFINE_SDOF_PROPERTIES* is used to specify the the properties of the moving zone, the valve disc, used by the SDOF-solver in FLUENT. These properties include the mass, inertia and weight load. The UDF is customized to prevent translation and to only allow rotation around the z-axis. A symmetry condition is used to take the symmetry of the model into account. Some additional commands are implemented to compute values of interest and pass them to other UDF:s. This macro was also used in the work by (Boqvist, 2013).

The UDF which uses the macro *DEFINE_EXECUTE_AT_END* writes the opening angle, angular velocity, angular acceleration and the torques of interest to a text file. This UDF is executed at the end of every time step and receives calculated data from the UDF using the macro *DEFINE_SDOF_PROPERTIES*.

The UDF which uses the macro *DEFINE_PROFILE* defines the inlet boundary condition by setting a starting velocity and a deceleration. The theoretical starting velocity, which is the lowest velocity at which the valve is at a fully open position, can be calculated by assuming equality between the static hydraulic torque and the torque caused by weight. Hence the theoretical starting velocity can be expressed as in Eq. 3.3.

$$C_{HS}\rho \mathrm{A}_v \frac{v^2}{2} L = T_w \quad \Rightarrow$$

$$v = \sqrt{\frac{2T_w}{C_{HS}\rho \mathrm{A}_v L}} \tag{3.3}$$

The stationary hydraulic torque coefficient C_{HS} will be available from steady state simulation with the valve disc fixed at 60 degrees. As the theoretical starting velocity is determined, it is slightly increased to assure that the valve disc stays fully open as the transient deceleration begins. The deceleration is supposed to simulate the velocity effects of pump stop. The deceleration is changed for different simulations to investigate the correlations between flow deceleration and closure behavior.

It is possible to implement other macros in UDF:s for controlling the motion of the valve, for example *DEFINE_CG_MOTION*. This macro specifies the motion of a dynamic zone by providing FLUENT with the linear and angular velocities at every time step. These properties can be calculated by determining the hydraulic forces in order to retrieve the resulting hydraulic torque. This torque is added to Newton's second law of motion to calculate the angular acceleration. The angular velocity is calculated by multiplying the angular acceleration with the time step. The velocity is used to update the node positions on the dynamic zones according to solid-body motion. This macro was used in the work by (Turesson, 2011).

3.4 Solver settings

For steady-state simulations, it is investigated which of the pressure-based solvers SIMPLE and Coupled handles these cases most accurate according to convergence and results. The pressure-based Coupled solver is considered due to its ability to reduce time in overall convergence for subsonic applications (Keating, 2011). The drawback of higher memory requirements will not be any problem in this work. SIMPLE is considered as pressure-velocity coupling solver due to its robustness and ability to converge. The algorithm uses a starting guess for pressure and velocity when solving the momentum equations. The initial guess will not satisfy continuity which introduces correction factors for pressure and velocity to improve the iterative solution. As velocity and pressure are corrected the remaining transport equations are solved. This is repeated until convergence is reached (Andersson et al., 2012).

The Coupled solver will be used for transient cases due to its advantages to handle strong coupled fluid–structure interaction cases (FSI). With advice from ANSYS Support the Coupled solver combined with the SDOF-solver, which handles the moving zones, should be a suitable approach. Solution stabilization is activated due to the possible solution sensitivity to data obtained through the system couplings. This setting is often beneficial for FSI problems in which the fluid is compressible according to the FLUENT v16 manual.

Both steady-state and transient simulations start off with first discretization order for momentum, pressure and turbulent properties during 25-50 iterations. The order of discretization is then switched to second order for momentum and pressure. This increases the magnitude of the residuals, however, the solution should be more accurate.

All steady-state simulations are initialized with the full-multigrid initialization option (FMG). The multigrid approach solves the flow problem on a sequence of coarser meshes, before transferring the solution onto the actual mesh. This initialization method provides the approximate solution at a minimum cost to overall computational expense. The method is more time consuming compared to standard and Hybrid initialization, however, a calculated solution should be provided much faster after FMG-initialization. The Hybrid solution initialization is used for all transient simulations. It contains a collection of methods to efficiently initialize the solution. It is only based on simulation setup which makes user input unnecessary (Keating, 2011). In FLUENT it is also possible to initialize a solution based on the solution from a previous similar case using interpolation. Even though different stationary cases is quite similar, this initializing method will not be used in this work with the advice of ANSYS Support.

3.5 Boundary conditions

The relevant boundaries which are in need of specified conditions in this flow problem is the inlet and outlet of the domain. The inlet is specified as velocity inlet which allows the user to specify the inlet velocity magnitude. This velocity is perpendicular to the boundary and constant during steady-state simulations and is controlled by an UDF during transient simulations. The velocities used in the stationary cases are $2, 4, 6$ and 8 m/s. The written UDF can be modified to control the initial inlet velocity and the deceleration as the transient simulation proceeds. The used dynamic velocities in the transient cases are presented in the following Tab. 3.2 and are intended to resemble different pump stop scenarios.

Table 3.2: Velocities and decelerations used in transient simulations.

Initial velocity $[m/s]$	**Deceleration** $[\mathbf{m/s^2}]$
3	-4
3	-6
3	-8
3	-10
3	-15

The pressure-outlet boundary condition is used for the outlet boundary. The gauge pressure is set to zero which implies that the absolute pressure in the domain in the same as the operating pressure, which is 1 atm by default. The pressure-outlet condition allows velocity variation on the boundary with zero pressure on the cell faces. All walls are impermeable and the no-slip condition is used.

3.6 Turbulence settings

FLUENT provide numerous different turbulence options which can be selected by the user. Settings related to turbulence in this work is limited to the turbulence intensity, choice of turbulence model, wall treatment and inflation layer sizing.

3.6.1 Turbulence boundary conditions

For both inlet- and outlet boundary condition, the turbulence is set to depend on the turbulence intensity and the hydraulic diameter, where the hydraulic diameter for a pipe is the same as the inner diameter. The turbulence intensity is defined as the ratio of the root-mean-square of the velocity fluctuations, u', to the mean flow velocity, u_{avg}. This relation can be expressed as a function of Reynolds number with respect to the hydraulic diameter derived from an empirical correlation for pipe flow for fully developed duct flow according to Eq. 3.4. The change in turbulent intensity is negligible for the different stationary velocities. Hence, the turbulent intensity used in all simulations is 2.5 %.

$$I = \frac{u'}{u_{avg}} = 0.16 Re_{dh}^{-1/8} \tag{3.4}$$

3.6.2 Turbulence models

The RANS-based turbulence models will be tested and evaluated according to their ability to yield stable converged solutions during a number of stationary simulations with a fixed valve disc. The most suitable turbulence model will then be used for all stationary simulations and also for all transient simulations. As mentioned in section 2.4.2, the impact of the following turbulence models will be investigated.

- Standard k-ϵ model
- Realizable k-ϵ model
- SST k-ω model

3.6.3 Inflation layer sizing

The prismatic inflation layers on the pipe- and valve walls are based on the dimensionless number y^+, which is the distance from the wall measured in viscous lengths, also called wall units (Pope, 2012). The value of y^+ of the different walls are determined through calculations with FLUENT. The average value of y^+ for each wall is used to set the first suitable cell height for the inflation layer. This is performed according to the approach by (LEAP CFD Team, 2013) which starts by determine the Reynolds number according to Eq. 3.5.

$$Re = \frac{\rho U D}{\mu} \tag{3.5}$$

Here, ρ is the density of the fluid, U is the velocity in the x-direction at the seat, D is the diameter of the pipe or the valve disc and μ is the dynamic viscosity of the fluid. Based on empirical results the Reynolds number is used to estimate the skin friction coefficient for internal flows (pipe flow) in Eq. 3.6 and for external flows (valve disc) in Eq. 3.7.

$$C_{f,i} = 0.079 Re^{-0.25} \tag{3.6}$$

$$C_{f,e} = 0.058 Re^{-0.2} \tag{3.7}$$

The skin friction coefficient is used to estimate the shear stress on the wall according to Eq. 3.8

$$\tau_w = \frac{1}{2} C_f \rho U^2 \tag{3.8}$$

The frictional velocity is a velocity scale for the near-wall region. It is calculated according to Eq. 3.9.

$$U_\tau = \sqrt{\frac{\tau_w}{\rho}} \tag{3.9}$$

The retrieved value of y^+ from FLUENT is used to determine the cell height of the cell on the wall surface by using Eq. 3.10.

$$y^+ = \frac{\rho U_\tau \Delta y_1}{\mu} \quad \Rightarrow \quad \Delta y_1 = \frac{y^+ \mu}{\rho U_\tau} \tag{3.10}$$

3.7 Model in RELAP5

The one-dimensional model used in RELAP5 is constructed to resemble the CFD-model used in FLUENT. The model consists of two time dependent volumes, both upstream and downstream. Between these time dependent volumes are two pipe segments, the swing check valve and two kinds of junctions connected. The time dependent junction specifies the incoming velocity of flow and the single junction connects the downstream pipe to the time dependent volume. Each pipe consists of 40 nodes with a specified node length of 0.1 meter. The swing check valve is modeled as a servo valve, which is a valve used in RELAP5 that can be implemented through user defined control variables. The theory of (Li and Liou, 2003) is set up by the implementation of these control variables. An illustration of the model used in RELAP5 is presented in Fig 3.5 as seen in the graphical interface SNAP, which is an abbreviation of Symbolic Nuclear Analysis Package.

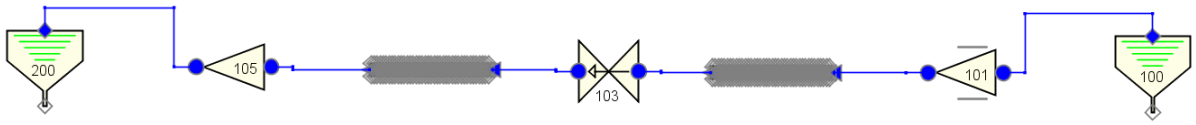

Figure 3.5: Schematic illustration in of model used in RELAP5.

4 Results and Discussion

This section starts with presenting results from the sensitivity analyses where the influence of mesh structure and settings in ANSYS FLUENT have been investigated. These results determines the most suitable model settings during the relevant CFD-simulations. The results from stationary simulations are then presented to show how these results differ from the final transient simulations. Written text files from the monitors in FLUENT contains saved data for quantities of interest as well as the text files from the UDF:s. The retrieved data have been transferred to MATLAB to produce graphic illustrations and to compile tables. All results are commented and discussed.

4.1 Sensitivity analysis

All simulations performed to investigate the sensitivity of mesh structure and choice of physics in FLUENT are based on stationary simulations. Sensitivity analysis regarding time step on the transient case would be a useful supplement, however it has been considered to be too time consuming.

4.1.1 Cell density

The sensitivity of the results due to cell density was tested in order to continue with a suitable and stable mesh during the simulations. The different cell densities used in the analysis is presented in Tab. 4.1 with the calculated stationary hydraulic torque coefficient.

Table 4.1: Amount of cells in domain with 60 degrees fixed opening angle.

Alternative	**Number of cells**	C_{HS}
1	795371	0.8379
2	1457261	0.8455
3	3515543	0.8468

Three different cell densities was used in the cell density study. The calculated stationary torque coefficient was reasonably unaffected for the different cell densities. The most suitable mesh to proceed with was alternative 2, with respect to computational time. Alternative 1 was not selected to proceed with, mainly due to the mesh interfaces where quantities are interpolated between the cell layers. The coarsest mesh showed obvious discontinuities in the interface region between the valve house and downstream pipe segment. The mesh in alternative 2 show no signs of discontinuities and will be used for all further stationary simulations. A quantitative illustration of the comparison at the mesh interface is presented in Fig. 4.1. Contour plots show the velocity magnitude in the x-direction just downstream of the valve housing. The results from the investigation of first inflation layer cell height is presented in section 4.1.6.

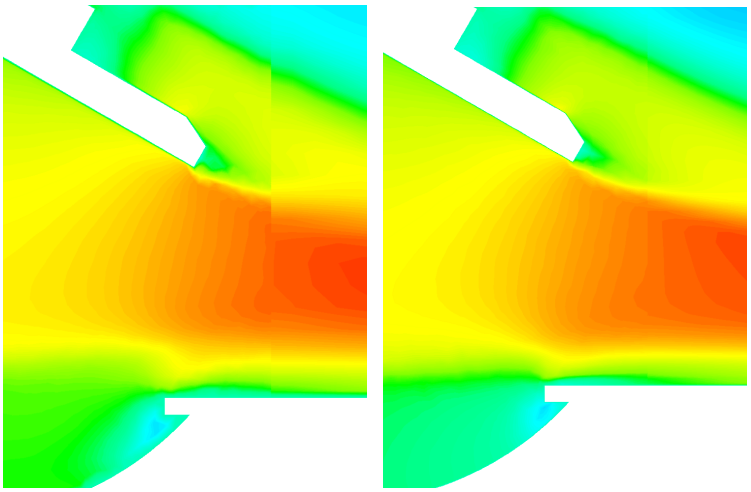

(a) Alternative 1 (b) Alternative 2

Figure 4.1: Velocity contours in the symmetry plane showing the discontinuity for the coarsest mesh at the interface compared with the second finest mesh.

It would be possible to use unstructured mesh for the whole domain in order to avoid the use of mesh interfaces. However, since the geometry for the pipes are uncomplicated it is suitable to use a structured mesh due to the advantages of low memory footprint, high order scheme applicability and speed of solution algorithms. The CFD-models by (Boqvist, 2013) and (Turesson, 2011) uses unstructured mesh for both pipe and valve house domain.

4.1.2 Solver dependence

As mentioned in section 3.4, the difference in results between the SIMPLE- and Coupled solver is investigated by comparing the calculated stationary hydraulic coefficient for a number of opening angles at an inlet velocity of 2 m/s. The results are presented in Tab. 4.2.

Table 4.2: Solver dependence on stationary torque coefficient.

Angle [°]	**SIMPLE** C_{HS} [-]	**Coupled** C_{HS} [-]	**Diff** [%]
60	0.8326	0.8260	0.79
50	1.5700	1.5554	0.93
40	2.0594	2.0666	0.35
35	2.2370	2,2374	0.02

Table 4.2 show that there is an negligible difference in chosen stationary torque coefficient results. However, the time to reach an acceptable level of convergence between the solutions was quite significant. As mentioned in (Keating, 2011), the Coupled solver was superior in time of convergence compared to the SIMPLE-solver. The Coupled solver yielded a converged solution after 100-300 iterations while the SIMPLE solver needed 1200-1800 iterations. The number of iterations are proportional to calculation time which was the main reason to proceed with the Coupled solver for all further calculations. The Coupled solver provided a converged solution after approximately 20 minutes, while the SIMPLE-solver provided a converged solution after approximately 1 hour and 30 minutes.

4.1.3 Reynolds dependency

The Reynolds dependency is investigated by comparing the stationary torque coefficient C_{HS} for different velocities. The presented result show C_{HS} for 30 degrees opening angle.

Table 4.3: Results from Reynolds dependency test for 30 degrees opening angle.

Reynolds number [-]	**Velocity [m/s]**	$\boldsymbol{C_{HS}}$ **[-]**
835980	2	2.4587
1671960	4	2.4486
2507940	6	2.4457
3343920	8	2.4457

There is a negligible difference between the stationary torque coefficient. This behavior covers all simulated opening angles which proves the Reynolds and velocity independence of the stationary torque coefficient. This makes it possible to estimate the coefficient and the corresponding stationary torque for all intermediate angles and velocities.

4.1.4 Complete geometry

Since the original model is cut in half using a symmetry plane, it is of interest to investigate if and how this approach affects the results compared to a full body model. The stationary torque coefficient is used as a comparative quantity since it is an important term used in the theory of (Li and Liou, 2003). Alternative 2 from the cell density analysis is used in this study. Hence the number of computational cells is approximately doubled to 3567947 cells.

Table 4.4: Effect of geometry regarding C_{HS}.

Angle [°]	**Half model** $\boldsymbol{C_{HS}}$ **[-]**	**Complete model** $\boldsymbol{C_{HS}}$ **[-]**	**Diff [%]**
60	0.8326	0.8019	3.69
50	1.5701	1.5516	1.18
40	2.0665	2.0483	0.88
30	2.4587	2.4195	1.59

The calculated stationary torque coefficient showed no obvious trend in difference between the symmetry model and the complete model. Obviously, the time for each iteration is approximately doubled. These results motivates to continue using the symmetry model through the rest of the simulations. The three-dimensional properties of turbulence should not be heavily affected with the half-model since the investigated models are all based on RANS. Table 4.5 show how different turbulence properties on a number of surfaces are affected by the choice of geometry. The investigated turbulent properties consist of the dimensionless wall distance y^+, turbulent viscosity ν_T and turbulent kinetic energy k. The results show small differences between the two geometric models. The largest difference is the turbulent viscosity at the interface surface just upstream of the valve housing. It is possible that the interpolation between the two mesh regions can be the cause of this difference.

Table 4.5: Comparison between turbulent properties for the half symmetry model and the complete model with a fixed opening angle of 60 degrees.

		Half model	**Complete model**	**Diff [%]**
y^+ [-]	Valve disc	39.7801	39.7610	0.0480
ν_T [kg/ms]	Outlet	1.6106	1.6129	0.1426
	Upstream	2.9002	2.9414	1.4007
	Seat	0.4676	0.4692	0.3410
	Interface	1.3326	1.4049	5.1463
k [m^2/s^2]	Outlet	0.0133	0.134	0.7463
	Upstream	0.0276	0.0288	4.1667
	Seat	0.0077	0.0078	1.2821
	Interface	0.1340	0.1393	3.8047

4.1.5 Turbulence modelling

The impact on results based on choice of turbulence model was investigated with steady-state simulations on stationary valve opening angle at 40 degrees. The behavior of convergence was monitored by observing torque and total pressure on the valve disc together with area-averaged shear stress on the valve disc. The impact of the following turbulence models was investigated.

- Standard k-ϵ model
- Realizable k-ϵ model
- SST k-ω model

The use of the Realizable k-ϵ model gave superior convergence behavior on all monitors and residuals. Since the solver is forced to find a steady-state solution, the Realizable k-ϵ model handles the recirculation zones in a more successful manner due to its ability to find an average solution. The use of all other turbulence models result in a diverging solution with highly fluctuating monitors. This can be explained by the physical nature of the problem where the flow field results and tends to behave as an unsteady and quite turbulent flow problem, probably due to the obvious recirculation- and separation zones near the valve disc. Similar results have been observed in the work of (Boqvist, 2013). Since the Realizable k-ϵ model by far provided a stable steady-state solution compared with the other turbulence models, this model will be used for all stationary and transient simulations.

4.1.6 Wall treatment

The sensitivity analysis regarding the choice of wall functions is presented in Tab. 4.6. The dimensionless wall distance y^+ has been compared for different surfaces and wall functions.

Table 4.6: Impact of wall treatment. The opening angle is fixed at 60 degrees.

Wall function	**Surface**	$\boldsymbol{y^+}$ [-]	$\boldsymbol{C_{HS}}$ [-]
Standard	Upstream pipe	51.2086	
	Downstream pipe	71.2916	
	Valve disc	49.9320	0.8451
Scalable	Upstream pipe	51.2093	
	Downstream pipe	71.5814	
	Valve disc	49.8672	0.8444
Enhanced	Upstream pipe	52.2273	
	Downstream pipe	72.9642	
	Valve disc	51.2405	0.8455

The y^+-values does not show any significant differences between the Standard and Scalable wall functions. The Enhanced wall treatment differs approximately 2 % on calculated y^+ compared to the other wall functions. The difference between the calculated stationary hydraulic torque coefficient is approximately

0.1 %. According to ANSYS Support, it should be most suitable to use the Enhanced wall treatment for this CFD-model since it uses a k-ϵ model. Hence, this wall treatment model was used for all stationary and transient cases.

The determination of the first layer cell height for all stationary cases was considered to be too comprising. Hence the first inflation layer height was determined from steady-state simulations for different velocities at a fixed opening angle of 30 degrees. The first layer length Δy_1 for the different surfaces is presented with the corresponding y^+-value. The number of cell layers was set to seven layers for all stationary simulations and three layers for all transient simulations in order to achieve the smallest possible opening angle.

Table 4.7: Calculated first layer cell height Δy_1.

Surface	$\boldsymbol{y^+}$ [-]	$\boldsymbol{\Delta y_1}$ **[mm]**
Upstream pipe	52.2273	0.7260
Downstream pipe	72.9642	1.0142
Valve disc	51.2405	0.5911

4.2 Stationary simulations

The results from the stationary simulations have all been derived from the symmetry model for a number of different opening angles. The fixed angles used in the simulations are 60, 50, 40, 35, 30, 25, 20, 15, 10 and 8 degrees.

4.2.1 Stationary hydraulic torque

The stationary hydraulic torque for forward and backward flow is presented in Fig. 4.2 and Fig. 4.3 as a function of angle and velocity. It can be seen that the torque increases rapidly for opening angles less than 15 degrees. It can also be seen that the stationary hydraulic torque is dependent of velocity and increases as this parameters is increased. It is negative for all angles during backward flow since the torque component acts in the clockwise direction.

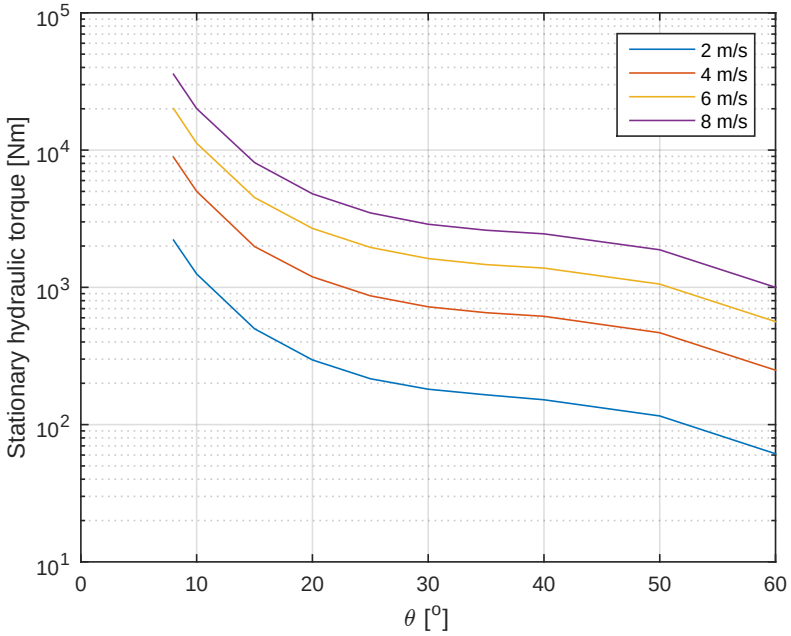

Figure 4.2: Stationary hydraulic torque as function of opening angle and velocity for forward flow

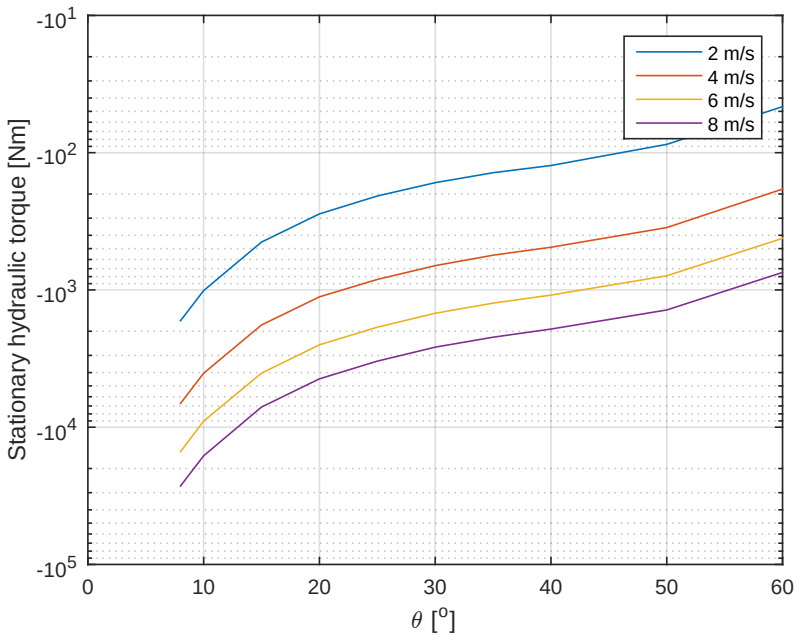

Figure 4.3: Stationary hydraulic torque as function of opening angle and velocity for backward flow.

The difference in stationary hydraulic torque between forward and backward flow is presented in Fig. 4.4. It is clear the torque component is larger for forward flow than for backward flow. The difference is minimized at fully opened position and at 25 degrees opening position. The differences are likely to depend on the geometry of the moving valve disc.

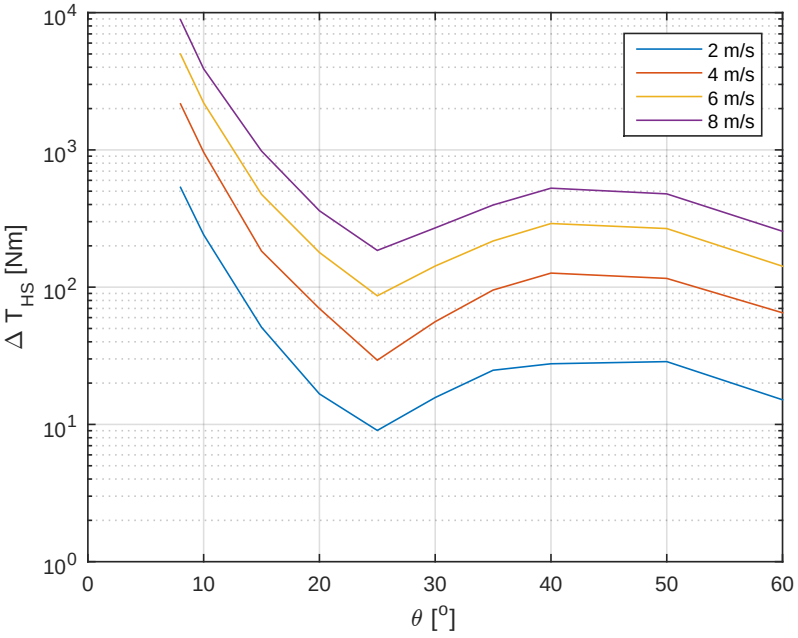

Figure 4.4: Difference in stationary hydraulic torque between forward and backward flow.

4.2.2 Stationary hydraulic torque coefficient

It was previously stated that the stationary torque coefficient C_{HS} should handle the angle dependency and act independent of velocity. The coefficient was calculated for forward and backward flow and is presented in Fig. 4.5 for 60, 40, 20 and 10 degrees opening angle.

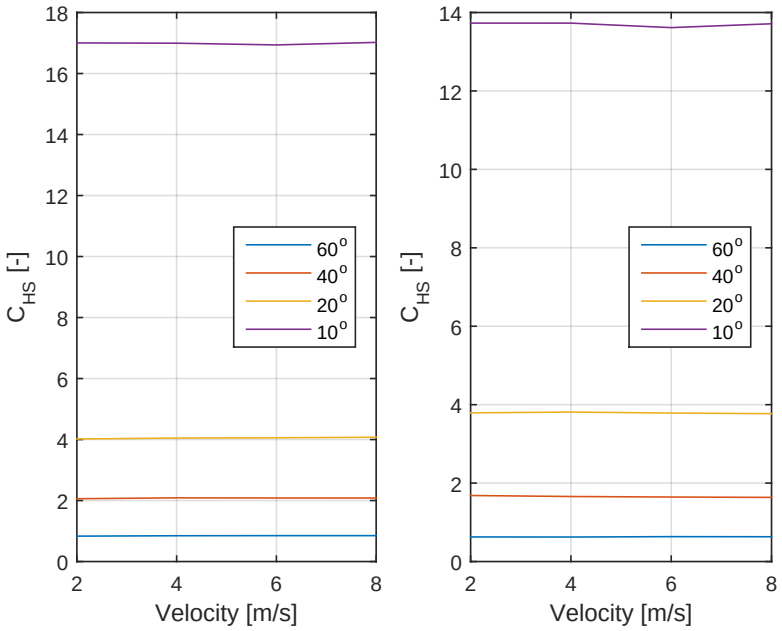

Figure 4.5: Left: C_{HS} for four different angles for forward flow. Right: C_{HS} for four different angles for backward flow.

It can be seen that the stationary torque coefficient is independent of velocity, both for forward and backward flow. The coefficient is however dependent on flow direction, possibly due to the geometry of the valve disc and rod. The stationary torque coefficient data is used to derive two functions with respect of opening angle, one for forward flow and one for backward flow. The functions are used to derive the stationary torque for intermediate angles from the total torque during the transient simulations. Since the coefficient is velocity independent of flow velocity, the stationary torque can be derived through an entire transient. As the direction of flow changes, the function is switched between forward- and backward flow function. The curve adjustments was more successful with the opening angle on logarithmic form. The resulting functions is presented in Eq. 4.1 and Eq. 4.2. A graphical presentation of the functions can be seen in Fig. 4.6. The curve adjustment was performed with the MATLAB commando *fminsearch* using the least squared error principle.

$$C_{HS\,forward} = 1513.0186 \cdot ln(\theta)^{5.3531} \tag{4.1}$$

$$C_{HS\,backward} = 798.3904 \cdot ln(\theta)^{4.8643} \tag{4.2}$$

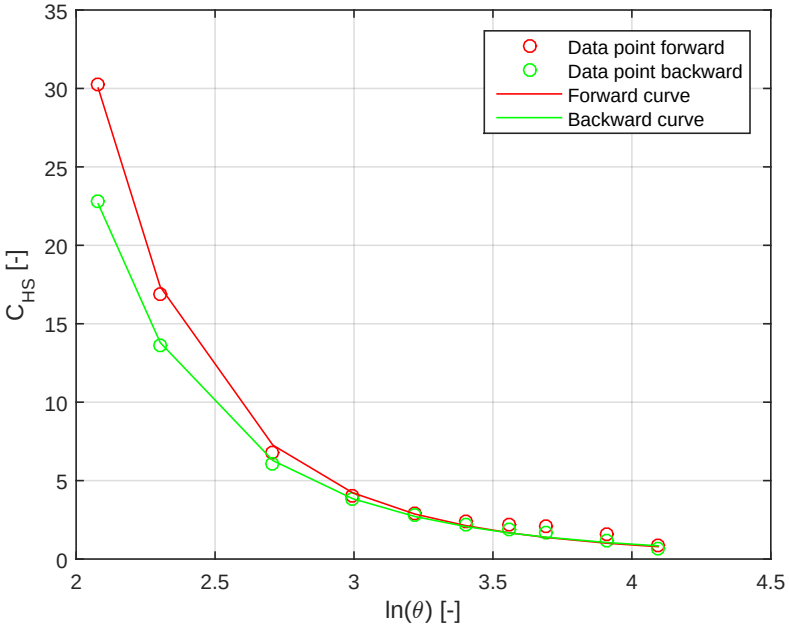

Figure 4.6: Function approximation with respect to data points from FLUENT.

The stationary hydraulic torque coefficient has also been derived as a function with respect the the static pressure loss. The static pressure loss increases with decreased opening angle and is presented in Fig. 4.7.

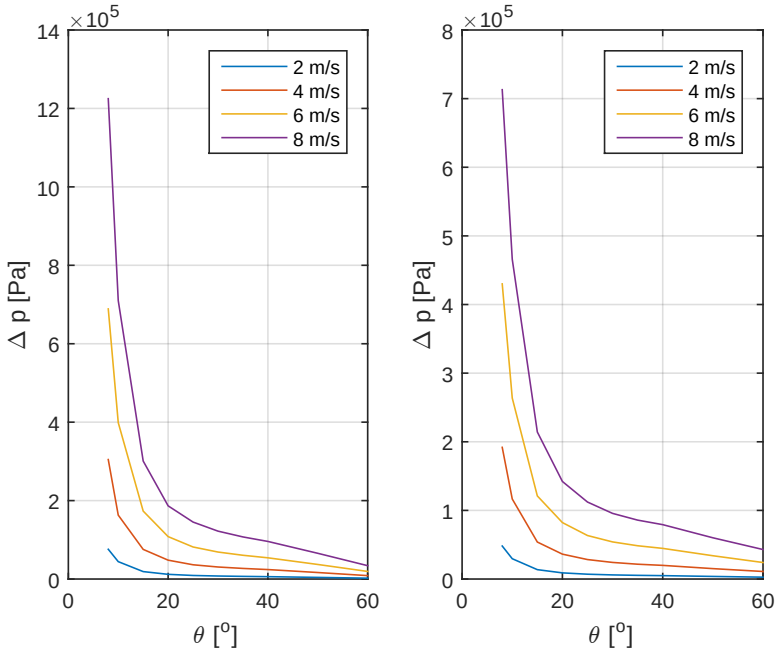

Figure 4.7: Left: Pressure loss as function of opening angle and velocity for forward flow. Right: Pressure loss as function of opening angle and velocity for backward flow.

The stationary torque coefficient is presented in Fig 4.8 as function of the differential pressure Δp. It can be seen that there is a linear correlation between C_{HS} and the pressure loss with differences depending on velocity.

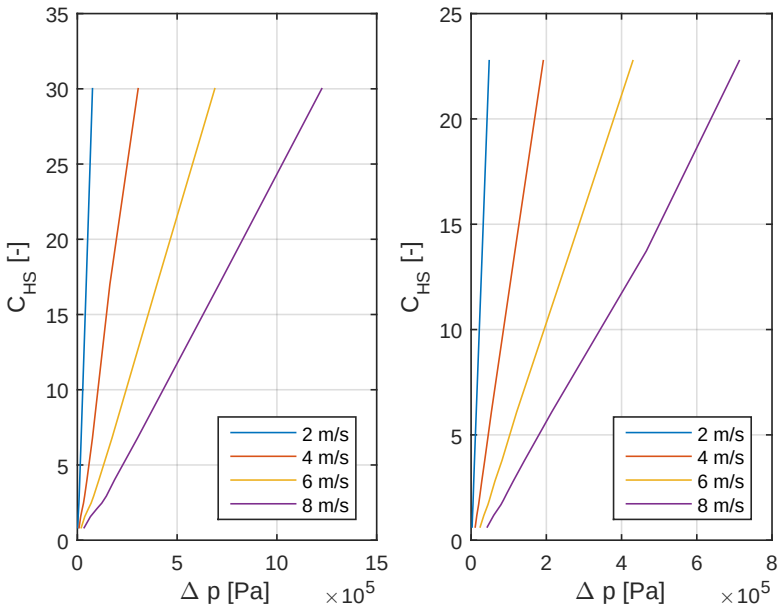

Figure 4.8: Left: C_{HS} as function of pressure loss and velocity for forward flow. Right: C_{HS} as function of pressure loss and velocity for backward flow.

4.3 Transient simulations

The transient simulations have provided the dynamic properties of the swing check valve model. These results can now be combined with the stationary in order to compare the results from CFD to the experimental results of (Li and Liou, 2003). The different transients was presented in Tab. 3.2. The dynamic results in terms of opening angle and angular velocity is presented for the different decelerations in Fig 4.9 and Fig. 4.10.

All transient curves in Fig. 4.9 have been translated in order to set the first time step of movement to the initial time. It can be seen that greater decelerations lead to faster closure. All transient simulations was executed with the same dynamic mesh settings. It is possible that the implicit mesh update interval should be increased for greater decelerations, especially during the the final degrees where the angular velocity is maximized. The closure progresses until approximately four degrees relative to a vertical positioned valve disc which correspond to an actual opening angle of approximately 1.5 degrees. Figure 4.10 show that the valve disc experiences an acceleration during the first ten degrees of closure. The angular velocity is then increased gradually until the valve disc starts to accelerate considerably towards the seat during the last 15-20 degrees.

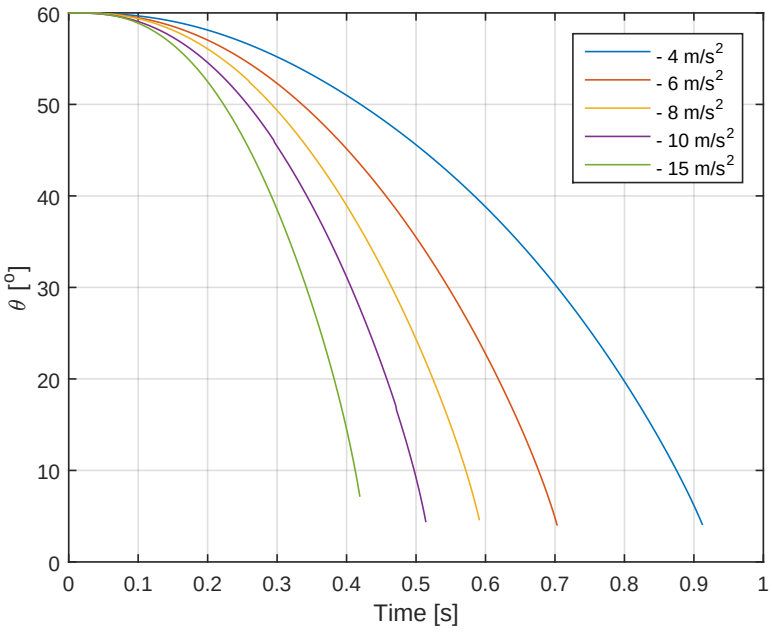

Figure 4.9: Opening angle as function of time during different transients.

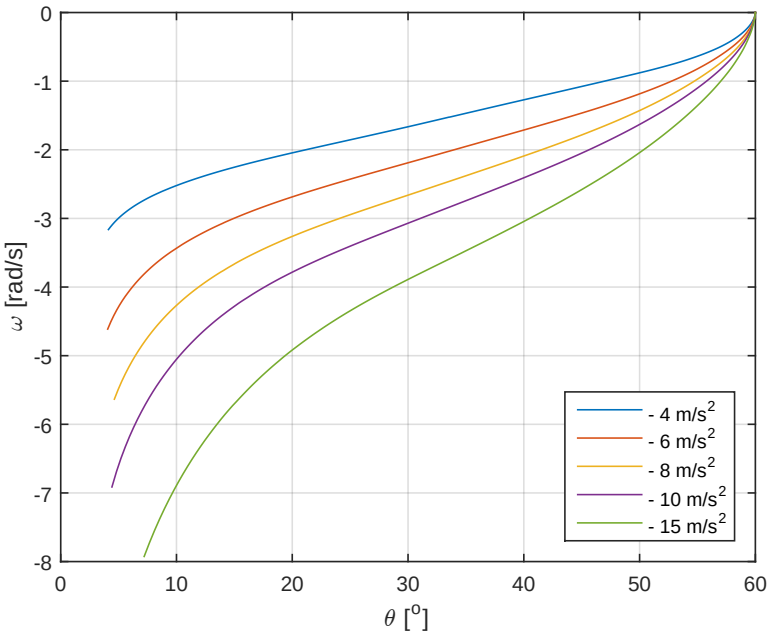

Figure 4.10: Angular velocity as function of angle during different transients.

The amount of back flow is approximated by summarizing the the massflow during each time step after the through flow has changed direction. The amount of back flow is presented in Tab. 4.8.

Table 4.8: Amount of back flow with respect to deceleration of flow.

Deceleration [m/s^2]	**Back flow [kg]**
-4	8.1779
-6	12.0770
-8	15.0337
-10	17.6487
-15	22.2251

4.3.1 Torque components

The rotational hydraulic torque was derived by subtracting the stationary torque from the total torque according to Eq. 2.14. The total hydraulic torque was provided by FLUENT during all entire transients and the stationary torque was derived using the stationary torque coefficient function for intermediate angles in Eq. 4.1 and Eq. 4.2. All torque components with respect to opening angle during one transient can be seen in Fig. 4.11. It can be seen that the two hydraulic torque components counteracts each other resulting in a net hydraulic torque. It can be seen that the stationary hydraulic torque changes sign as the through flow changes from forward flow to backward flow. The rotational hydraulic torque is positive during the entire transients due to the fact that the valve disc never rotates in clockwise direction. The rotational hydraulic torque acts as a breaking torque since the torque is positive during the closure motion.

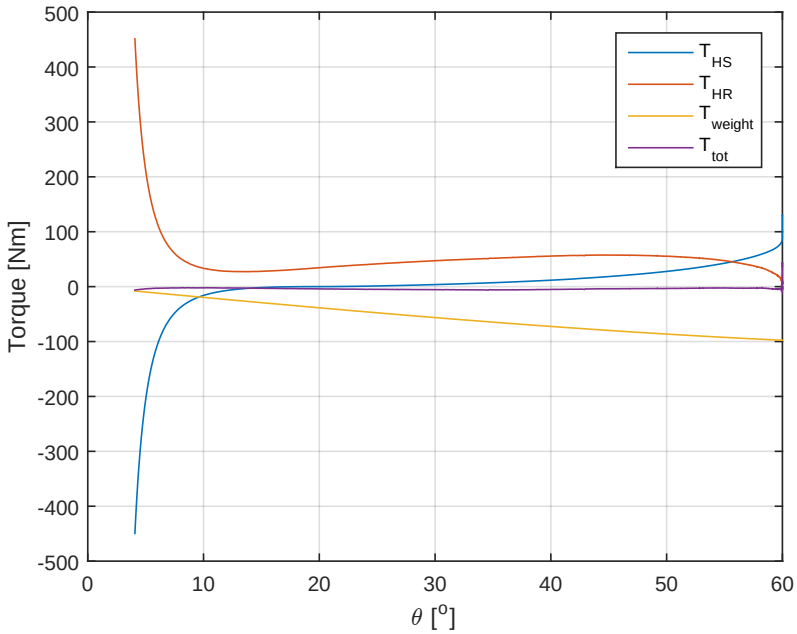

Figure 4.11: All torque components as function of angle during a deceleration of -4 m/s^2.

Figure 4.12 shows the corresponding results from the experiments by (Li and Liou, 2003). Great similarities can be seen for the stationary- and rotational hydraulic torque components compared to the results from CFD in Fig. 4.11. The large differences in torque magnitude can be explained by the large difference in valve sizing where the valve disc used in the experiments only has 3.2 % of the area compared the valve disc used in CFD.

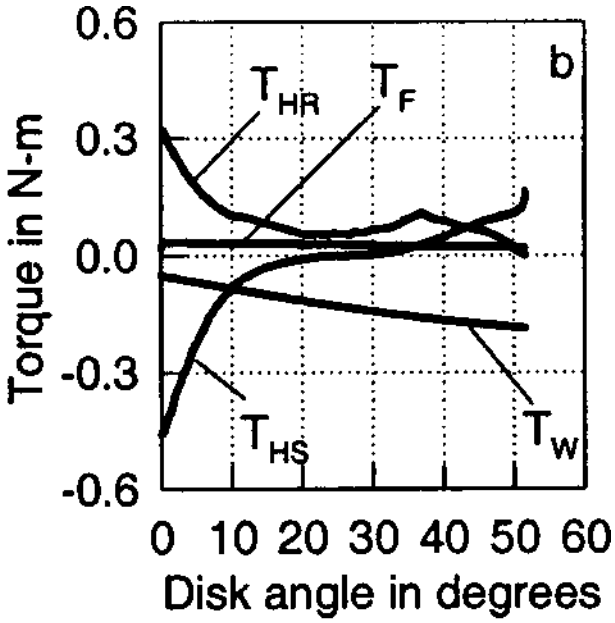

Figure 4.12: All torque components as function of angle from the experiments of (Li and Liou, 2003)

4.3.2 Rotational hydraulic torque coefficient

The rotational hydraulic torque coefficient is calculated according to Eq. 2.21 and is presented in Fig 4.13. It can be seen that the rotational hydraulic coefficient approaches high values for large opening angles. This is due to set-up of the transient model where the valve disc is held in an fully opened position with no angular velocity. As the disc starts to rotate and accelerate towards the seat, the coefficient decreases due to the increased angular velocity.

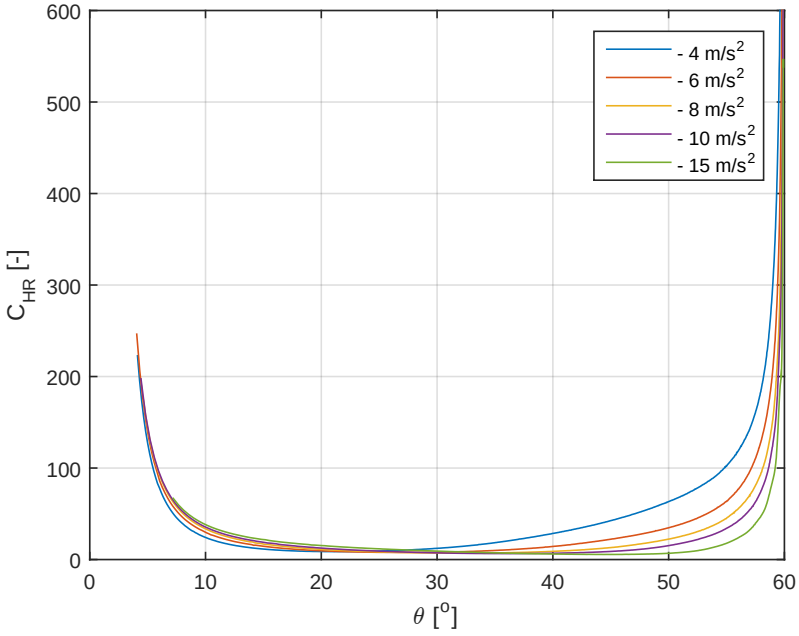

Figure 4.13: Rotational hydraulic torque coefficient C_{HR} as function of opening angle and deceleration.

The rotational hydraulic coefficient was said to be dependent on angular velocity. This can be seen in Fig. 4.14 for different decelerations. The coefficient is maximized for small angular velocities since $\dot{\theta}$ is located in the denominator in Eq. 2.21. The coefficient starts to decrease at a certain angular velocity depending

on deceleration. Each transient has a maximized angular velocity at the last time step, just before the seat. It can be seen in both Fig. 4.13 and Fig. 4.14 that the rotational hydraulic coefficient is maximized in that position.

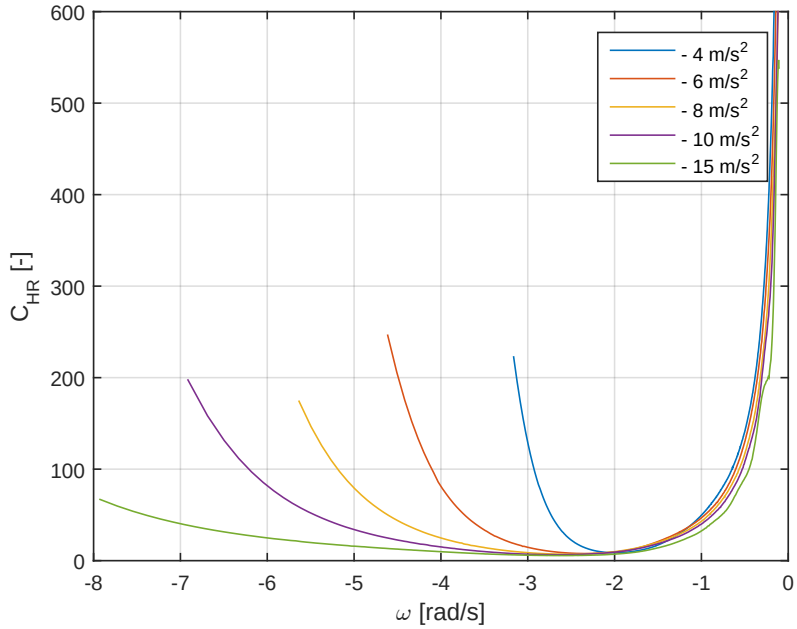

Figure 4.14: Rotational hydraulic torque coefficient C_{HR} as function of angular velocity and deceleration.

It has been investigated if there is a correlation between the two hydraulic coefficients. Figure 4.15 reveals that there is a linear correlation between the coefficients with relatively small differences between the the different decelerations during almost the entire transient. The difference is smaller between larger decelerations. The rotational hydraulic coefficient increases towards infinity for small values of the stationary hydraulic coefficient, which corresponds to a slowly moving valve disc starting at a fully opened position in the beginning of a transient deceleration.

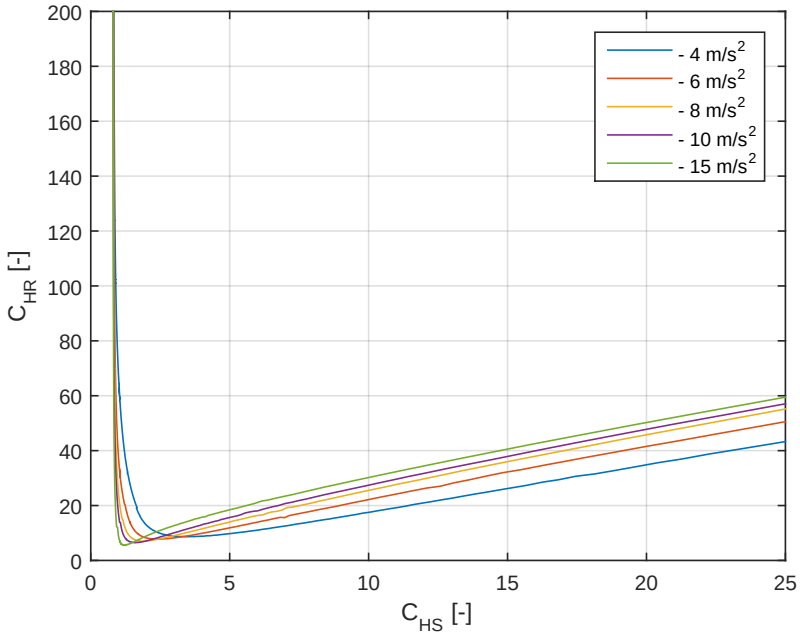

Figure 4.15: Rotational hydraulic torque coefficient C_{HR} as function of stationary hydraulic torque coefficient C_{HS} and deceleration.

The linear correlation between the coefficients can be used to derive linear equations where the slope k and intersection m are functions of deceleration $\frac{dv}{dt}$. Small values of C_{HS} has to be neglected in order to implement Eq. 4.3.

$$y = kx + m$$

$$C_{HR} = k(\frac{dv}{dt})C_{HS}(\theta) + m(\frac{dv}{dt}) \tag{4.3}$$

4.4 Results from RELAP5

The retrieved results from FLUENT was implemented in RELAP5, where the closure with respect to time has been derived for the same transients used in FLUENT. The valve is set to be either fully opened or fully closed and closes instantaneous as the calculated opening angle is zero. The through flow is controlled by the deceleration of flow which will affect the motion of the valve disc. The coefficients k and m are implemented with respect to the deceleration through tables, where RELAP5 linearly interpolates between values. The same procedure is used to retrieve the correct value of the stationary hydraulic torque coefficient with respect to opening angle, which makes it possible to derive the rotational hydraulic coefficient according to Eq. 4.3.

The results are presented in Fig. 4.16 and in Tab. 4.9. The corresponding closure from RELAP5 differs from the intervals presented in Fig. 4.11 where the closure is faster in the CFD-model for slower transients and slower for fast transient. This inconsistent behavior might be a sign of inferior implementation in RELAP5 since the results from CFD showed clear correlation between magnitude of deceleration and closing time. The curves for lower decelerations in Fig. 4.16 indicate a clear deviation as the valve disc is positioned between 10 and 15 degrees open.

It has previously been stated that the rotational hydraulic coefficient increases towards infinity for low angular velocities which yields a large rotational hydraulic torque component which has been assumed to dampened the closing motion. This behaviour has been neglected in RELAP5 due to the complexity of approximation of the coefficient for large opening angles. Hence, the valve disc does not encounter the same magnitude of breaking torque as the disc starts to move. This might be an explanation for the faster closing transients in RELAP5, however, it does not explain the slower closing time for faster transients.

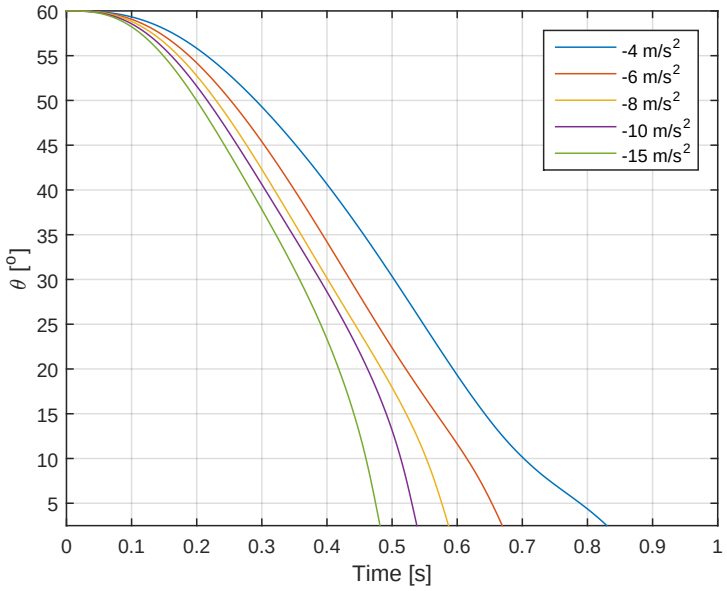

Figure 4.16: Opening angle with respect to time for different decelerations in RELAP5.

Table 4.9: Difference in closing time between swing check valve model used in FLUENT and RELAP5.

Transient [m/s^2]	**CFD** [s]	**RELAP5** [s]	**Diff** [%]
-15	0.425	0.488	-14.82
-10	0.517	0.545	-5.42
-8	0.605	0.596	1.49
-6	0.713	0.682	4.35
-4	0.938	0.828	11.73

4.5 Pressure and pressure surge

Simulations in FLUENT never captured any pressure surges in the system. The area-averaged static pressure monitors showed large oscillations during the first 20 % of each transient where the pressure eventually stabilized at an negative pressure relative to the operating pressure. All stationary simulations reached a steady-state static pressure for the corresponding cross sections in the domain. From this, it was possible to derive functions for stationary pressure loss and corresponding loss coefficient for all opening angles. However, due to the inability to retrieve static pressure field during transient simulations, it was not possible to compare these quantities between stationary and transient situation. The transient pressure loss characteristics would also be of use for valve implementation in RELAP5.

The transient pressure results are difficult to describe with a physical explanation. Hence they might be a result due to mesh structure and mesh settings. The dynamic boundary condition for the inlet was constructed in a similar approach as in the work of (Turesson, 2011) and (Boqvist, 2013) where the inlet velocity is changing with time due to a fixed deceleration. This boundary condition itself is unphysical since the magnitude of velocity sets the pressure. The velocity of a real flow is a result of pressure difference, not the opposite.

Since the valve disc is unable to fully close it was not possible to bring the through flow to rest by fully blocking the flow path. This might be an important issue to handle if pressure surges are to be captured during valve closure. FLUENT provides settings which are designed to handle contact between dynamic surfaces where an UDF is used to provide nodal contact information. These settings are called contact detection settings and are included in the dynamic mesh section.

5 Conclusions

It is possible to implement the swing check valve theory of (Li and Liou, 2003) in CFD-simulations and retrieve data for all important hydraulic components. However, it is a complex matter to generate a general one-dimensional swing check valve model based on three-dimensional CFD-simulations. This is mainly due to the dependency of the coefficients which are used to describe the hydraulic torque. In addition, simulations should be performed on similar valves with different geometric properties in order to find correlations due to size, inertia etc.

It is possible to use a symmetry model for simulations of swing check valve. Results show negligible differences for the calculated stationary hydraulic torque coefficient and torque results between the symmetry model and full body model. This approach saves computational time due to reduced amount of computational cells. It is important to accurately set up the dynamic mesh properties in order to successfully create the dynamic zones, both in the bulk region and in the symmetry plane.

It is important to distinguish the stationary flow progress from a fully transient simulation. Quasi-stationary simulations can only give useful results for different stationary cases which differs greatly from time dependent transient cases.

6 Future work

The results from the CFD-simulations has provided data which has been used to derive some useful correlations with respect to the theory of (Li and Liou, 2003). However, to be able to create a more general one-dimensional model based on this theory, future work should be repeated for different swing check valves with differences in geometric properties in order to gather a large amount of data which could be used to map in the one-dimensional model. Similar approaches have been performed for pumps. Common schematic pump curves often present the head with respect to volume flow. It is possible to derive pump efficiency and power for different operation modes using the pump curve. The common pump curve often provided by the manufacturer only present the pump characteristics for one of four possible quadrants representing the combinations of positive and negative head and volume flow. The characteristics for the other three quadrants can be investigated by experiments or mapped in, based on other pumps with all known quadrants. A similar approach could be possible for the swing check where the approach used in this work is tested for different valves. This might yield useful correlations between geometric properties and the hydraulic torque components and their coefficients.

As mention in section 2.3, pressure surges can occur during pipe rupture, which is a rapid transient compared to pump stops. It would be of interest to simulate this phenomena using CFD with a governing pressure based inlet boundary condition. This boundary condition would effect the flow in a short period of time, reducing the inlet pressure from several bars of pressure to atmospheric pressure. One challenge would be how to set up and handle the dynamic mesh movement during this fast transient. The valve disc would most likely intend to close fast which probably would require a vast number of iterations per time step along with several iterative mesh updates in order to avoid negative cell volumes and simulation crash. As mention in section 4.5, this boundary condition is physical correct compared to the the boundary condition used in this work, where velocity determines the pressure.

If a swing check valve of smaller size should be implemented in CFD, the frictional torque could be of importance according to (Li and Liou, 2003). The frictional torque could be implemented by using an expression for frictional torque in a UDF which is used by FLUENT when solving equation of rotating motion.

It would be of interest using ANSYS FLUENT's volume of fluid (VOF) multiphase modeling capability to study the effects of column separation as a result of valve closure. Hence it is of importance to be able to fully close the valve at the end of the transient in order to capture a column separation.

Bibliography

Andersson, B., R. Andersson, L. Håkansson, M. Mortensson, R. Sudiyo, and B. Van Wachem. *Computational Fluid Dynamics for Engineers*. Cambridge University Press, Cambridge, UK, 2012.

Boqvist, E. Investigation of a swing check valve using CFD. Master's Thesis, Linköpings Universitet, Tekniska Högskolan, 581 83, Linköping, 2013.

Davis, P.L., A.T. Rinehimer, and M. Uddin. A Comparison of RANS-Based Turbulence Modeling for Flow over a Wall-Mounted Square Cylinder, 2012. URL `http://www.cd-adapco.com/technical_document/comparison-rans-based-turbulence-modeling-flow-over-wall-mounted-square-cylinder`. [Accessed March 25, 2015].

Douglas, J.F., J.M. Gasiorek, J.A. Swaffield, and L.B. Jack. *Fluid Mechanics - 5th edition*. Pearson Education Limited, Harlow, England, 2005.

DYVRO, . *Dokumentation für das Rechenprogramm DYVRO Mod. 3*. 2012.

KAE, . *DRAKO - Users Manual*. Kraftwerks- Anlagen- Engineering GmbH, Am Bauhof 4b D-91088 Bubenreuth, Germany, 3.22 edition, January 2005.

Keating, M. Accelerating cfd solutions. *ANSYS Advantage*, 5(1):48–49, 2011.

KSB, . Water Hammer. *KSB Know-How*, 1, 2006.

LEAP CFD Team, . Estimating the First Cell Height for correct y^+, 2013. URL `http://www.computationalfluiddynamics.com.au/tips-tricks-cfd-estimate-first-cell-height/`. [Accessed March 16, 2015].

Li, G. and J.C.P Liou. Swing Check Valve Characterization and Modeling During Transients. *Journal of Fluids Engineering*, 125(10):1043–1050, 2003.

McElhaney, K.L. An Analysis of Check Valve Performance Characteristics Based on Valve Designs. *Nuclear Engineering and Design*, (197):169–182, 2000.

Nyberg, C. *Mekanik Fortsättningskurs*. Liber, Liber AB, 113 98 Stockholm, 2010.

Pandula, Z. and G. Halász. Dynamic Model for Simulation of Check Valves in Pipe Systems. *Periodica Polytechnica Ser. Mech. Eng.*, 46(2):91–100, 2002.

Pope, S.B. *Turbulent Flows*. Cambridge University Press, Cambridge, UK, 2012.

The RELAP5-3D© Code Development Team, . *RELAP5-3D© Code Manual Volume I: Code Structure, System Models, and Solution Methods*. Southpointe, 2005.

Thorley, A.R.D. Check valve behavior under transient flow conditions: A state-of-the-art review. *Journal of Fluids Engineering*, 111(2): , 1989.

Tu, J., G. Yeoh, and C. Liu. *Computational Fluid Dynamics - A Practical Approach*. Elsevier Ltd, Oxford, UK, 2008.

Tullis, J.P. *Hydraulics in Pipelines*. John Wiley & Sons, Inc, Hoboken, New Jersey, 1989.

Turesson, M. Dynamic simulation of check valve using CFD and evaluation of check valve model in RELAP5. Master's thesis, Chalmers University of Technology, Department of Chemistry and Bioscience, SE-412 96 Göteborg, 2011.

Young, Donald F., Bruce R. Munson, Theodore H. Okiishi, and Wade W. Huebsch. *A Brief Introduction to Fluid Mechanics*. John Wiley Sons, Inc, 2007.

Zappe, R.W. and P. Smith. *Valve selection Handbook*. Elsevier Science Publishers, Burlington, USA, 2004.

Záruba, J. *Water Hammer in Pipe-Line Systems*. Elsevier Science Publishers, Amsterdam, The Netherlands, 1993.

A UDF used in ANSYS FLUENT

The following UDF contains the three macros which have been presented in section 3.3.

```
#include "udf.h"
#include "f_wall.h"
#include "dynamesh_tools.h"

static real torque_tot,torque_hyd, torque_w, theta, omega, alpha;

DEFINE_SDOF_PROPERTIES(motion, prop, dt, time, dtime)
{
        Domain *domain = Get_Domain(1);
        Thread *thread = Lookup_Thread(domain,29);

        real L_cg[3], force[3], moment[3];
        NV_S(L_cg,=,0);
        NV_S(force,=,0);
        NV_S(moment,=,0);

        Compute_Force_And_Moment(domain,thread,L_cg,force,moment,TRUE);

        prop[SDOF_MASS] = 6.6125e-3*(8030.0-998.2);
        prop[SDOF_IYY] = 1;
        prop[SDOF_IXX] = 1;
        prop[SDOF_IZZ] = 3.863;
        prop[SDOF_ZERO_TRANS_X] = TRUE;
        prop[SDOF_ZERO_TRANS_Y] = TRUE;
        prop[SDOF_ZERO_TRANS_Z] = TRUE;
        prop[SDOF_ZERO_ROT_X] = TRUE;
        prop[SDOF_ZERO_ROT_Y] = TRUE;
        prop[SDOF_ZERO_ROT_Z] = FALSE;
        prop[SDOF_SYMMETRY_X] = 0;
        prop[SDOF_SYMMETRY_Y] = 0;
        prop[SDOF_SYMMETRY_Z] = 1;

        /*Adding weight torque to total torque.
        Minus sign - negative defined angle */
        prop[SDOF_LOAD_M_Z] = -9.81*prop[SDOF_MASS]
        *0.2473*sin(DT_THETA (dt)[2] + 60*M_PI/180);

      /*Total torque - doubled due to symmetry*/
        torque_tot = (2*moment[2] + prop[SDOF_LOAD_M_Z]);
        /*Hydrualic torque - doubled due to symmetry*/
        torque_hyd = 2*moment[2];
        /*Weight torque*/
        torque_w = prop[SDOF_LOAD_M_Z];
        /*Opening angle*/
        theta = DT_THETA(dt)[2];
```

```
        /*Angular velocity*/
        omega = DT_OMEGA_CG(dt)[2];
        /*Angular acceleration*/
        alpha = torque_tot/prop[SDOF_IZZ];

                /*If opening angle is equal or greater than 0 (60 degrees)
                and net torque is larger than 0 => Hold disk position.
                If opening angle is smaller than -57 (3 degrees) =>
                 => Hold disk position  */

                if((DT_THETA(dt)[2] >= 0 && torque_tot > 0)
                || (DT_THETA(dt)[2] <= -0.99483767)){
                        prop[SDOF_ZERO_ROT_Z] = TRUE;
                        printf ("Fully open / closed ");
                }
                else
                {
                        prop[SDOF_ZERO_ROT_Z] = FALSE;
                }
              node_to_host_real_1(torque_tot);
                node_to_host_real_1(torque_hyd);
                node_to_host_real_1(torque_w);
                node_to_host_real_1(theta);
                node_to_host_real_1(omega);
                node_to_host_real_1(alpha);
}

DEFINE_EXECUTE_AT_END(results)
{
 #if !RP_HOST

 int i;
 FILE *fp_torque;
 FILE *fp_theta;

 #if PARALLEL
  if(I_AM_NODE_ZERO_P)
 #endif
  {
   if(!(fp_torque=fopen("torque_results.txt","a")))
     {
       Message0("\nCan not open file-aborting!!");
       exit(0);
     }
   if(!(fp_theta=fopen("theta_results.txt","a")))
     {
       Message0("\nCan not open file-aborting!!");
       exit(0);
     }
  }


#if PARALLEL
  if(I_AM_NODE_ZERO_P)
#endif
  {
   fprintf(fp_torque, "%12.4e ", CURRENT_TIME);
   fprintf(fp_theta, "%12.4e ", CURRENT_TIME);
```

```
  fprintf(fp_torque, "%12.4e %12.4e %12.4e ",
  torque_tot, torque_hyd, torque_w );
  fprintf(fp_theta, "%12.4e %12.4e %12.4e ",
  theta, omega, alpha);
  fprintf(fp_torque, "\n");
  fprintf(fp_theta, "\n");
  fclose(fp_theta);
  fclose(fp_torque);
 }

#endif
}

DEFINE_PROFILE(inlet_velocity, thread, position)
{
        face_t f;
        real t = CURRENT_TIME;
        begin_f_loop(f, thread)
        {
        if (t < 0.01)
                F_PROFILE(f, thread, position) = 3; /* m/s */
        else
                F_PROFILE(f, thread, position) = 3-4*(t-0.01); /* m/s */
        }
        end_f_loop(f, thread)
}
```